Depth-averaged equations for compressible shallow-water flows and tsunamis

Gaël Loïc Richard

▶ **To cite this version:**

Gaël Loïc Richard. Depth-averaged equations for compressible shallow-water flows and tsunamis. 2020. hal-02959509

HAL Id: hal-02959509
https://hal.inrae.fr/hal-02959509

Preprint submitted on 6 Oct 2020

HAL is a multi-disciplinary open access archive for the deposit and dissemination of scientific research documents, whether they are published or not. The documents may come from teaching and research institutions in France or abroad, or from public or private research centers.

L'archive ouverte pluridisciplinaire **HAL**, est destinée au dépôt et à la diffusion de documents scientifiques de niveau recherche, publiés ou non, émanant des établissements d'enseignement et de recherche français ou étrangers, des laboratoires publics ou privés.

HAL
archives-ouvertes.fr

Depth-averaged equations for compressible shallow-water flows and tsunamis

G. L. Richard

▶ **To cite this version:**

G. L. Richard. Depth-averaged equations for compressible shallow-water flows and tsunamis. 2020. hal-02959509

HAL Id: hal-02959509
https://hal.inrae.fr/hal-02959509

Preprint submitted on 6 Oct 2020

HAL is a multi-disciplinary open access archive for the deposit and dissemination of scientific research documents, whether they are published or not. The documents may come from teaching and research institutions in France or abroad, or from public or private research centers.

L'archive ouverte pluridisciplinaire **HAL**, est destinée au dépôt et à la diffusion de documents scientifiques de niveau recherche, publiés ou non, émanant des établissements d'enseignement et de recherche français ou étrangers, des laboratoires publics ou privés.

Depth-averaged equations for compressible shallow-water flows and tsunamis

Gaël L. Richard*[1]

[1]Univ. Grenoble Alpes, INRAE, UR ETNA, 38000 Grenoble, France

Abstract

A new system of equations is derived for compressible shallow-water flows with a depth-averaging method and a weak-compressibility assumption. The variations of the depth-averaged density are due to the variations of the hydrostatic pressure caused by depth variations. The obtained system of four equations is fully nonlinear, hyperbolic and admits an exact conservation of energy on an arbitrary bathymetry as well as on a mild-slope bottom. The dispersive properties are consistent with the linear theory of compressible fluids at the long-wave limit. The equations include the possibility of a mobile bottom, enabling the simulation of tsunamis generated by seabed vertical movements. A system with improved dispersive properties is presented with accurate velocities for all tsunamis wavelengths. The solutions of the dispersive relation divide into a slow branch governing gravity waves and a rapid branch governing acoustic waves. The numerical scheme is based on a splitting between a slow part treated explicitly and a fast part solved implicitly but without any global linear system to solve. The numerical resolution of a one-dimensional tsunami generated by vertical bottom movements shows the decrease of the tsunami velocity due to compressible effects and a later arrival time than in an incompressible case.

1 Introduction

Boussinesq-type models are commonly used for water waves simulations if the shallow-water – or long-wave – assumption holds, which is the case for coastal waves or for tsunami propagation. The original Boussinesq model (Boussinesq 1872) was derived for a constant depth. It was extended by Peregrine (1967) to the case of a variable bathymetry. The Boussinesq model is weakly nonlinear, which means that the nonlinearity parameter, defined by a/h where a is the wave amplitude and h the water depth, is small. This assumption entails some discrepancies, notably in the case of coastal waves where the nonlinearity can increase to $O(1)$. A fully nonlinear model was first derived by Serre (1953) (see also Su & Gardner 1969) in the one-dimensional (1D) case and extended to the two-dimensional (2D) case by Green and Naghdi (Green *et al.* 1974, Green & Naghdi 1976). This model, called thereafter the Serre-Green-Naghdi model, can be derived from the Euler equations as an asymptotic model in the shallow-water regime without any assumption on the wave amplitude (Lannes 2013). Even if they are fully nonlinear, the shallow water hypothesis (the depth is small compared to the wavelength) implies that these models are weakly dispersive (see for example Kirby 2016). The dispersion relation of the Airy wave theory is recovered if $kh \ll 1$ where k is the wave number. Many works were proposed aiming at extending the validity domain of the Boussinesq-type models to larger depths or shorter wavelengths with respect to their dispersive properties (Madsen & Sørensen 1992, Nwogu 1993, Wei *et al.* 1995, Kennedy *et al.* (2001), Bonneton *et al.* 2011, Chazel *et al.* 2011). The reader

*Corresponding author: gael.richard@inrae.fr

is referred to Brocchini (2013) and Kirby (2016) for a complete review of the Boussinesq-type models.

The Boussinesq-type models can be derived by averaging over the water depth the equations of fluid mechanics. As a result, the dimension of the system is reduced by one; a 2D-flow is modelled by a 1D-system of equations and a three-dimensional (3D) flow reduces to a 2D-model. Furthermore the boundary conditions at the bottom and at the free surface are incorporated in the model equations. The computational time for a numerical simulation is thus greatly reduced. However the numerical resolution is confronted with two important problems. The first problem is the presence of high-order derivatives in the equations which are not easy to handle numerically. In particular, the Serre-Green-Naghdi equations feature third-order derivatives, and some Boussinesq-type models with improved dispersive properties include fifth-order derivatives. The second problem is that an elliptic step has to be solved at each time step of the numerical resolution. Both problems result from the assumption of incompressibility which creates a non-local effect since pressure variations propagate at an infinite celerity in an incompressible fluid. The pressure satisfies an elliptic Poisson equation which is the mathematical expression of this non-locality. In the depth-averaged models of the Boussinesq-type, the non-locality entails also an elliptic step which is time-consuming because a global linear system has to be solved at each time step. Moreover the resolution of the linear system adds complexity for the implementation of parallelization techniques which are often necessary to reduce the computation time.

A solution of these problems was first obtained by Favrie & Gavrilyuk (2017) who derived a hyperbolic approximation of the Serre-Green-Naghdi equations for a constant bathymetry with a variational method using an augmented Lagrangian leading to an unconditionally hyperbolic system giving the Serre-Green-Naghdi system when a parameter of the new system goes to infinity. This method reduces greatly the computational time. A mathematical justification of this approximation was given by Duchêne (2019). Another hyperbolic approximation was derived by Escalante *et al.* (2019) for an arbitrary bathymetry with the method of an artificial compressibility. This approach was extended by Escalante & Morales de Luna (2019) who obtained a hyperbolic approximation covering several classical Boussinesq-type models. The hyperbolic system may be seen as a relaxation of the original non-hyperbolic system. It is based on a modified system in which the divergence constraint on the velocity field is coupled with the other conservation laws and, in particular, with a transport equation for the non-hydrostatic pressure, including a relaxation term on the depth-averaged vertical velocity which introduces a high but finite velocity. At the limit where this velocity goes to infinity, the original non-hyperbolic system is recovered.

These approaches are related to the general method of taking into account the compressibility and the propagation of acoustic waves in order to avoid the resolution of a global system at each time step. This method is used in atmospheric numerical models for a long time (see for example Hill 1974, Klemp & Wilhelmson 1978, Skamarock & Klemp 1992, 2008) and in non-hydrostatic ocean models (Auclair *et al.* 2018). The drawback of this method is that the very high value of the sound velocity (around 1500 $\mathrm{m}\cdot\mathrm{s}^{-1}$ in water) severely restricts the time step. This problem can be solved by using an artificially smaller sound velocity, adding thus an artificial compressibility, leading to a system which is sometimes called pseudo-compressible (Auclair *et al.* 2018). The same method is used for the hyperbolic approximations of the Boussinesq-type models where the large parameter giving the original non-hyperbolic system at the infinite limit is chosen as small as possible to give the same results as the incompressible system at an excellent approximation while keeping the time step to a reasonably small value.

In these approaches the compressibility and the acoustic waves are not included for themselves but to facilitate and accelerate the numerical resolution. The hyperbolic models were conceived as hyperbolic approximations of the incompressible non-hyperbolic Serre-Green-Naghdi or Boussinesq-type models. The goal was to obtain nearly the same solutions with a hyperbolic

structure to remove the high-order derivatives and the elliptic step. Compressible effects are for most cases negligible because of the usually very small value of the Mach number. However compressibility can have measurable effects in the case of tsunamis. Standard models for tsunami propagation predict arrival times which are systematically too early compared to the observations. The delay is significative and can reach several minutes in the far field (see for example Yamazaki *et al.* 2012, Grilli *et al.* 2012, in the case of the 2011 Tohoku-oki event). This discrepancy is attributed to two main effects which are the compressibility of seawater and the elasticity of the solid earth (Tsai *et al.* 2013, Allgeyer & Cumins 2014, Baba *et al.* 2017, Abdolali & Kirby 2017). Although a tsunami in a deep ocean is still a shallow-water flow since the order of magnitude of its wavelength (about 100 km) is much larger than the ocean depth (4 000–6 000 m), the Mach number defined by the ratio of the incompressible surface wave celerity $\sqrt{gh}$, where g is the gravity acceleration, to the sound speed is of the order of 0.13–0.16 which leads to a decrease of the phase speed by about 0.5 % (Abdolali *et al.* 2019) which can explain an important part of the observed discrepancy. Various methods have been implemented to take into account this compressibility effect and the earth elasticity effect (Tsai *et al.* 2013, Allgeyer & Cummins 2014, Watada 2014, Baba *et al.* 2017, Abdolali & Kirby 2017, Abdolali *et al.* 2019).

In this paper a depth-averaged model is derived. This model is fully nonlinear and of the Boussinesq-type except that it is hyperbolic and that it includes compressibility effects on dispersive properties and wave velocities. The Serre-Green-Naghdi model and its hyperbolic approximation are a particular case of this more general compressible model when the Mach number goes to zero. The static compressibility of the ocean is taken into account. In §2 the model is derived in the case of a constant depth. The energy conservation, hyperbolicity and dispersive properties are studied. The soliton solutions are studied in §3. The numerical resolution with an implicit-explicit (IMEX) numerical scheme is presented in §4 in the case of the propagation of a soliton. The model on an arbitrary topography, including a mobile bottom, is derived in §5. In §6 it is shown numerically that the model is able to capture the diminution of the speed of a tsunami due to the compressibility of seawater.

2 Equations in the case of a constant depth

2.1 Governing equations

In this part the depth is constant. The extension to an arbitrary bathymetry and a mobile bottom is studied in §5. We study the propagation of waves in an inviscid compressible fluid with a density ρ and a pressure p. The horizontal coordinate is x (unit vector $\boldsymbol{e_x}$) and the vertical coordinate is z (unit vector $\boldsymbol{e_z}$) such that the bottom is at $z = 0$ and the free surface at $z = h(x, t)$. The components of the fluid velocity field $\boldsymbol{v}$ are u in the Ox-direction and w in the Oz-direction. The continuity equation can be written

$$\frac{\partial \rho}{\partial t} + \frac{\partial \rho u}{\partial x} + \frac{\partial \rho w}{\partial z} = 0. \tag{1}$$

The gravity acceleration is denoted by $\boldsymbol{g} = -g\boldsymbol{e_z}$. The momentum balance equation in the Ox and Oz-directions are respectively

$$\frac{\partial \rho u}{\partial t} + \frac{\partial \rho u^2}{\partial x} + \frac{\partial \rho uw}{\partial z} = -\frac{\partial p}{\partial x} \tag{2}$$

and

$$\frac{\partial \rho w}{\partial t} + \frac{\partial \rho uw}{\partial x} + \frac{\partial \rho w^2}{\partial z} = -\rho g - \frac{\partial p}{\partial z}. \tag{3}$$

The boundary condition at the bottom reduces to the no-penetration condition

$$w(0) = 0. \tag{4}$$

The kinematic boundary condition at the free surface can be written

$$w(h) = \frac{\partial h}{\partial t} + u(h)\frac{\partial h}{\partial x}. \tag{5}$$

The surface tension being neglected, the dynamic boundary condition at the free surface states that the pressure at $z = h$ is equal to the atmospheric pressure, which is supposed to be a constant that can be taken equal to zero. This leads to

$$p(h) = 0. \tag{6}$$

Since the fluid is compressible, the mass and momentum equations are not sufficient to close the problem. The first law of thermodynamics and an equation of state must be added to describe completely the system. Previous works suggest that density stratification due to temperature or salinity variations have much smaller effects than the increase of ocean water density with depth due to the seawater compressibility in the gravity field (Tsai *et al.* 2013, Watada 2013). Note that bottom friction has a negligible effect in deep oceans, in particular on tsunami delay (Watada 2014, Allgeyer & Cummins 2014). The following assumptions can be made: 1) The flow is homentropic i.e. the entropy s is uniform and constant; 2) The fluid is barotropic; 3) The sound velocity, denoted by a, is uniform and constant. The same hypotheses were assumed by most authors. Consequently the equation of state is taken as

$$p = a^2 \left(\rho - \rho_s\right) \tag{7}$$

where ρ_s is the seawater density at the free surface. It is of course also possible to write the well-known formula

$$\frac{\partial p}{\partial \rho} = a^2. \tag{8}$$

In the absence of heat transfer, the first law of thermodynamics can be written

$$\frac{\partial}{\partial t}\left(\frac{1}{2}\rho v^2 + \rho g z + \rho e_i\right) + \operatorname{div}\left[\left(\frac{1}{2}\rho v^2 + \rho g z + \rho e_i + p\right)\boldsymbol{v}\right] = 0 \tag{9}$$

where e_i is the specific internal energy. In the case of a homentropic flow ($\mathrm{d}s = 0$), the thermodynamic relation $\mathrm{d}e_i = T\mathrm{d}s + (p/\rho^2)\mathrm{d}\rho$ (with T being the temperature) reduces to

$$\mathrm{d}e_i = \frac{p}{\rho^2}\mathrm{d}\rho. \tag{10}$$

In the absence of waves, the ocean is supposed to be in hydrostatic equilibrium. The quantities evaluated in this state are denoted by a subscript 0. By definition the equilibrium hydrostatic pressure p_0 is related to the equilibrium density ρ_0 by

$$\frac{\partial p_0}{\partial z} = -\rho_0 g. \tag{11}$$

In these conditions, the equation of state writes $p_0 = a^2(\rho_0 - \rho_s)$. The integration of (11) gives the basic hydrostatic ocean state (Abdolali & Kirby 2017)

$$\rho_0 = \rho_s \mathrm{e}^{g(h_0 - z)/a^2} \tag{12}$$

where h_0 is the still water depth. The expression of the pressure is then

$$p_0 = a^2\rho_s\left[\mathrm{e}^{g(h_0-z)/a^2}-1\right]. \tag{13}$$

When a wave propagates in the ocean, this equilibrium hydrostatic state is perturbed. This perturbation can be divided into two effects: a hydrostatic perturbation due to the variation of the water depth while the hydrostatic equation is still satisfied in the vertical direction (although not in the horizontal directions) and a non-hydrostatic effect induced by the vertical acceleration i.e. the left-hand side of (3). The pressure is thus written as the sum of a hydrostatic term p_H and a non-hydrostatic term p_N as

$$p = p_H + p_N. \tag{14}$$

The hydrostatic term is the sum of the equilibrium hydrostatic state and a hydrostatic perturbation

$$p_H = p_0 + \delta p_H. \tag{15}$$

To the non-hydrostatic pressure corresponds a density fluctuation ρ_N such that $p_N = a^2\rho_N$ and to the hydrostatic pressure corresponds a hydrostatic term ρ_H in the density with

$$\rho = \rho_H + \rho_N \tag{16}$$

and $p_H = a^2(\rho_H - \rho_s)$. By definition, the hydrostatic pressure is defined by

$$\frac{\partial p_H}{\partial z} = -\rho_H g, \tag{17}$$

which gives

$$\rho_H = \rho_s \mathrm{e}^{g(h-z)/a^2} \tag{18}$$

and

$$p_H = a^2\rho_s\left[\mathrm{e}^{g(h-z)/a^2}-1\right]. \tag{19}$$

Defining the water elevation by $\eta = h - h_0$, the hydrostatic density is related to its equilibrium value by the relation

$$\rho_H = \rho_0\,\mathrm{e}^{g\eta/a^2}. \tag{20}$$

Despite the term "static", the hydrostatic pressure p_H depends on the time t and on the abscissa x in the presence of a wave, through the altitude $h(x,t)$ of the free surface. The non-hydrostatic correction p_N is small in a shallow-water flow (see §2.2). The density perturbation due to the non-hydrostatic effects is also small. Denoting by $E_i = \rho e_i$ the internal energy per unit volume, E_i can be expanded as

$$E_i = E_{iH} + \left.\frac{\mathrm{d}E_i}{\mathrm{d}\rho}\right|_H \rho_N + \frac{1}{2}\left.\frac{\mathrm{d}^2E_i}{\mathrm{d}\rho^2}\right|_H \rho_N^2 + ... \tag{21}$$

where the subscripts H refer to the hydrostatic state. This development is inspired by the methods used in acoustics (see Myers 1986 for a purely acoustic study in the absence of body forces). The various expressions in the hydrostatic state can be written $E_{iH} = \rho_H e_{iH}$,

$$\left.\frac{\mathrm{d}E_i}{\mathrm{d}\rho}\right|_H = e_{iH} + \frac{p_H}{\rho_H} \tag{22}$$

and

$$\left.\frac{\mathrm{d}^2E_i}{\mathrm{d}\rho^2}\right|_H = \frac{a^2}{\rho_H}. \tag{23}$$

The specific internal energy in the hydrostatic case can be obtained from the thermodynamic relation (10) and the equation of state (7). The integration of

$$\frac{\mathrm{d}e_{iH}}{\mathrm{d}\rho_H} = a^2 \frac{\rho_H - \rho_s}{\rho_H^2} \tag{24}$$

leads to

$$e_{iH} = a^2 \ln \frac{\rho_H}{\rho_s} + a^2 \left(\frac{\rho_s}{\rho_H} - 1 \right), \tag{25}$$

taking the constant of the internal energy at the free surface equal to zero. Using the expression (18) yields the expression of the internal energy per unit volume

$$E_i = \rho_s g \left(h - z\right) \mathrm{e}^{g(h-z)/a^2} + a^2 \rho_s \left[1 - \mathrm{e}^{g(h-z)/a^2}\right] + g \left(h - z\right) \rho_N + \frac{a^2}{2\rho_s} \mathrm{e}^{-g(h-z)/a^2} \rho_N^2. \tag{26}$$

2.2 Scaling and dimensionless equations

The model is derived under the assumption of a shallow water flow, which is valid even for a tsunami in a deep ocean. Denoting by h_0 a characteristic depth and by L a characteristic length of the flow in the Ox-direction, the problem admits a a small parameter

$$\varepsilon = \frac{h_0}{L} \ll 1. \tag{27}$$

The model is derived with an asymptotic method. The equations are thus written in a dimensionless form to evaluate the order of magnitude of each term with respect to the small parameter ε.

Denoting by u_0 a characteristic horizontal fluid velocity, the Froude number is defined as $F = u_0/\sqrt{gh_0}$. For a tsunami in deep oceans F can be very small. However no assumption is made on the order of magnitude of F (i.e. $F = O[1]$) in order to derive a more general model. The following scaling for x, z, h, t, u, w is classical in the shallow water context (a tilde denotes a dimensionless quantity):

$$\tilde{x} = \frac{x}{L}\ ; \quad \tilde{z} = \frac{z}{h_0}\ ; \quad \tilde{h} = \frac{h}{h_0}\ ; \quad \tilde{t} = t\frac{F\sqrt{gh_0}}{L}\ ; \quad \tilde{u} = \frac{u}{F\sqrt{gh_0}}\ ; \quad \tilde{w} = \frac{w}{\varepsilon F\sqrt{gh_0}}\ ; \tag{28}$$

The Mach number is defined with the incompressible surface waves celerity as

$$M = \frac{\sqrt{gh}}{a}. \tag{29}$$

The Mach number in the equilibrium state is $M_0 = \sqrt{gh_0}/a$. Its order of magnitude must be estimated with respect to ε. Even if the compressibility is taken into account in this model, the fluids considered here are weakly compressible and therefore the Mach number is small. As there is no reason for the Mach number to be an integer power of ε, it is written

$$M_0 = \varepsilon^\gamma M_1, \tag{30}$$

where $0 < \gamma \leqslant 1$ and $M_1 = O(1)$. In practice, only the square of the Mach number occurs in the equations. Since $M_0^2 = O(\varepsilon^{2\gamma})$ with $0 < 2\gamma \leqslant 2$, if an integer power of ε is absolutely wanted, it is possible to choose $\gamma = 1/2$ and thus $M_0^2 = O(\varepsilon)$ or $\gamma = 1$ and $M_0^2 = O(\varepsilon^2)$.

Shearing effects, due to the variation of the horizontal fluid velocity in the depth, can be important nearshore, especially in the case of breaking, but in the deep ocean where the compressibility can have a measurable effect, they are negligible. There is no difficulty to include

shearing in the model in the same way as in Kazakova & Richard (2019) but in the present study it is not important and it is omitted to simplify the presentation. Therefore the order of magnitude of shearing effects will be chosen to be able to neglect them consistently in the equations. Denoting by U the depth-averaged horizontal velocity and $u' = u - U$ the deviation of the horizontal velocity with respect to this average value, u' is supposed to be small and to scale with $\varepsilon^\beta F\sqrt{gh_0}$ such that $\tilde{u} = \tilde{U} + \varepsilon^\beta \tilde{u}'$ with $\beta > 1$. This approach is due to Teshukov (2007) who considered the case $0 < \beta < 1$ to include explicitly shearing effects but not the dispersive terms whereas β is here greater than 1 to neglect the shearing terms but to include the dispersive terms. This approach can be also related to the vorticity. If the vorticity $\omega = \partial u/\partial z - \partial w/\partial x$ is of $O(\varepsilon^\alpha)$, then $\beta = \min(\alpha, 2)$ since, defining $\varepsilon^\alpha F\tilde{\omega} = \omega\sqrt{h_0/g}$, we have $\varepsilon^\alpha\tilde{\omega} = \varepsilon^\beta \partial\tilde{u}'/\partial\tilde{z} - \varepsilon^2\partial\tilde{w}/\partial\tilde{x}$. In the irrotational case, which is often an assumption for the study of tsunami propagation in deep ocean (see for example Abdolali & Kirby 2017), $\beta = 2$.

The pressure and density are scaled as in the incompressible case, with the surface density ρ_s as reference density,

$$\tilde{\rho} = \frac{\rho}{\rho_s}\ ; \quad \tilde{p} = \frac{p}{\rho_s g h_0}. \tag{31}$$

The dimensionless mass and momentum balance equations in the Ox and Oz directions become respectively

$$\frac{\partial\tilde{\rho}}{\partial\tilde{t}} + \frac{\partial\tilde{\rho}\tilde{u}}{\partial\tilde{x}} + \frac{\partial\tilde{\rho}\tilde{w}}{\partial\tilde{z}} = 0, \tag{32}$$

$$\frac{\partial\tilde{\rho}\tilde{u}}{\partial\tilde{t}} + \frac{\partial\tilde{\rho}\tilde{u}^2}{\partial\tilde{x}} + \frac{\partial\tilde{\rho}\tilde{u}\tilde{w}}{\partial\tilde{z}} = -\frac{1}{F^2}\frac{\partial\tilde{p}}{\partial\tilde{x}}, \tag{33}$$

and

$$\varepsilon^2F^2\left(\frac{\partial\tilde{\rho}\tilde{w}}{\partial\tilde{t}} + \frac{\partial\tilde{\rho}\tilde{u}\tilde{w}}{\partial\tilde{x}} + \frac{\partial\tilde{\rho}\tilde{w}^2}{\partial\tilde{z}}\right) = -\tilde{\rho} - \frac{\partial\tilde{p}}{\partial\tilde{z}}. \tag{34}$$

Taking into account the definition of the hydrostatic pressure (17), the last equation can be reduced to

$$\varepsilon^2F^2\left(\frac{\partial\tilde{\rho}\tilde{w}}{\partial\tilde{t}} + \frac{\partial\tilde{\rho}\tilde{u}\tilde{w}}{\partial\tilde{x}} + \frac{\partial\tilde{\rho}\tilde{w}^2}{\partial\tilde{z}}\right) = -\tilde{\rho}_N - \frac{\partial\tilde{p}_N}{\partial\tilde{z}}. \tag{35}$$

which shows that $p_N = O(\varepsilon^2F^2)$. The dimensionless non-hydrostatic pressure is thus redefined as

$$\tilde{p}_N = \frac{p_N}{\varepsilon^2F^2\rho_s g h_0} \tag{36}$$

This gives the relation $\tilde{p} = \tilde{p}_H + \varepsilon^2F^2\tilde{p}_N$, showing that the non-hydrostatic pressure is a small correction to the pressure. From $p_N = a^2\rho_N$ we deduce that

$$\tilde{\rho}_N = \varepsilon^{2+2\gamma}M_1^2F^2\tilde{p}_N \tag{37}$$

which implies that the perturbation to the density due to the non-hydrostatic pressure is very small (of $O[\varepsilon^3]$ if $2\gamma = 1$ or of $O[\varepsilon^4]$ if $2\gamma = 2$). In the incompressible limit, p_N is also of $O(\varepsilon^2)$ with $\rho_N = 0$, which is possible given that $a \to \infty$ (or $M_0 = 0$). In the weakly compressible approach, the non-hydrostatic pressure keeps the same order of magnitude with a large but finite sound velocity (or a small but non-zero Mach number) and a very small density perturbation. The definition of $\tilde{\rho}_N$ is thus changed into

$$\tilde{\rho}_N = \frac{\rho_N}{\varepsilon^{2+2\gamma}F^2\rho_s} \tag{38}$$

and $\tilde{\rho}_N = M_1^2\tilde{p}_N$. With this new scaling for p_N and ρ_N, the equation (35) becomes

$$\frac{\partial\tilde{\rho}\tilde{w}}{\partial\tilde{t}} + \frac{\partial\tilde{\rho}\tilde{u}\tilde{w}}{\partial\tilde{x}} + \frac{\partial\tilde{\rho}\tilde{w}^2}{\partial\tilde{z}} = -\varepsilon^{2\gamma}\tilde{\rho}_N - \frac{\partial\tilde{p}_N}{\partial\tilde{z}}. \tag{39}$$

The corrective term on the weight due to the non-hydrostatic effect is thus small and it can be consistently ignored given that all other terms are already of $O(\varepsilon^2)$, writing

$$\frac{\partial \tilde{\rho}\tilde{w}}{\partial \tilde{t}} + \frac{\partial \tilde{\rho}\tilde{u}\tilde{w}}{\partial \tilde{x}} + \frac{\partial \tilde{\rho}\tilde{w}^2}{\partial \tilde{z}} = -\frac{\partial \tilde{p}_N}{\partial \tilde{z}} + O\left(\varepsilon^{2\gamma}\right). \tag{40}$$

The dimensionless form of the equation of state restricted to the leading hydrostatic part of the pressure is

$$\tilde{p}_H = \frac{\tilde{\rho}_H - 1}{\varepsilon^{2\gamma} M_1^2}. \tag{41}$$

This implies that $\tilde{\rho}_H = 1 + O(\varepsilon^{2\gamma})$. The weak compressibility implies that the density differs only slightly from its surface value ρ_s. However this difference is not negligible since the dispersive non-hydrostatic terms which are taken into account are of $O(\varepsilon^2)$. This difference ρ' is defined as $\rho_H = \rho_s + \rho'$ and scaled as $\tilde{\rho}' = \rho'/(\varepsilon^{2\gamma}\rho_s)$. In dimensionless form, we have

$$\tilde{\rho}_H = 1 + \varepsilon^{2\gamma}\tilde{\rho}'. \tag{42}$$

It follows that the mass conservation equation (32) can be written

$$\frac{\partial \tilde{u}}{\partial \tilde{x}} + \frac{\partial \tilde{w}}{\partial \tilde{z}} + \varepsilon^{2\gamma}\left(\frac{\partial \tilde{\rho}'}{\partial \tilde{t}} + \frac{\partial \tilde{\rho}'\tilde{u}}{\partial \tilde{x}} + \frac{\partial \tilde{\rho}'\tilde{w}}{\partial \tilde{z}}\right) = O\left(\varepsilon^{2+2\gamma}\right). \tag{43}$$

The first two terms are the leading incompressible terms. The following terms of $O(\varepsilon^{2\gamma})$ are the compressible hydrostatic correction and the right-hand side of $O(\varepsilon^{2+2\gamma})$ is the neglected compressible non-hydrostatic correction. In the same way, the horizontal momentum balance equation writes

$$\frac{\partial \tilde{\rho}_H\tilde{u}}{\partial \tilde{t}} + \frac{\partial \tilde{\rho}_H\tilde{u}^2}{\partial \tilde{x}} + \frac{\partial \tilde{\rho}_H\tilde{u}\tilde{w}}{\partial \tilde{z}} + \frac{1}{F^2}\frac{\partial \tilde{p}_H}{\partial \tilde{x}} + \varepsilon^2\frac{\partial \tilde{p}_N}{\partial \tilde{x}} = O\left(\varepsilon^{2+2\gamma}\right) \tag{44}$$

where the hydrostatic perturbation $\tilde{\rho}'$ is included in $\tilde{\rho}_H$, giving terms of $O(\varepsilon^{2\gamma})$.

2.3 Depth-averaged equations

2.3.1 Depth-averaged quantity

The governing equations are averaged over the depth. For any quantity A, its depth-averaged value for a compressible fluid can be defined in two ways. The first average, denoted by $\langle A\rangle$, is the depth-average counterpart of the Favre averaging and is defined as

$$\langle A\rangle = \frac{\displaystyle\int_0^h \rho A \,\mathrm{d}z}{\displaystyle\int_0^h \rho \,\mathrm{d}z}. \tag{45}$$

The second average is denoted by $\overline{A}$ and is the usual depth average

$$\overline{A} = \frac{1}{h}\int_0^h A \,\mathrm{d}z. \tag{46}$$

Since $\rho = \rho_H + \varepsilon^{2+2\gamma}F^2\rho_N$, the first average can be written

$$\langle A\rangle = \frac{\displaystyle\int_0^h \rho_H A \,\mathrm{d}z}{\displaystyle\int_0^h \rho_H \,\mathrm{d}z} + O\left(\varepsilon^{2+2\gamma}\right). \tag{47}$$

Introducing the normalized depth-averaged hydrostatic density $R = \overline{\rho_H}/\rho_s$ leads to the following relations in dimensional and dimensionless forms

$$\int_0^h \rho_H A \,\mathrm{d}z = \rho_s h R \langle A \rangle \;\; ; \quad \int_0^{\tilde{h}} \tilde{\rho}_H \tilde{A} \,\mathrm{d}\tilde{z} = \tilde{h} R \langle \tilde{A} \rangle. \tag{48}$$

The following notations are used for the average fluid horizontal velocity, for the average fluid vertical velocity (both being of the Favre type) and for the normalized average non-hydrostatic pressure: $U = \langle u \rangle$, $W = \langle w \rangle$ and $P = \overline{p_N}/\rho_s$ (which gives $\tilde{P} = \overline{\tilde{p}_N}$ in dimensionless form with $P = \varepsilon^2 F^2 g h_0 \tilde{P}$). From the definition $u = U + u'$, it follows that $\langle u' \rangle = 0$. This implies also that $\overline{\tilde{u}} = \tilde{U} + O(\varepsilon^{\beta+2\gamma})$. In the case of the horizontal fluid velocity, the difference between the two averages is negligible if $\gamma > 1/2$ or if $\beta = 2$ (irrotational flow). In the case of the fluid vertical velocity, $\tilde{W} = \overline{\tilde{w}} + O(\varepsilon^{2\gamma})$.

The expression of the average density R can be found from the integration of (18) which yields

$$R = \frac{\mathrm{e}^{M^2} - 1}{M^2}. \tag{49}$$

Since the Mach number is small, the development of this expression can be restricted to

$$R = 1 + \frac{M^2}{2} + O(M^4). \tag{50}$$

2.3.2 Mass conservation

With the above definitions, and taking into account the kinematic boundary condition, the integration of the mass conservation equation over the fluid depth gives

$$\frac{\partial \tilde{h} R}{\partial \tilde{t}} + \frac{\partial \tilde{h} \tilde{U} R}{\partial \tilde{x}} = O(\varepsilon^{2+2\gamma}). \tag{51}$$

This equation can be written

$$\left(R + \tilde{h} \frac{\mathrm{d}R}{\mathrm{d}\tilde{h}} \right) \left(\frac{\partial \tilde{h}}{\partial \tilde{t}} + \frac{\partial \tilde{h} \tilde{U}}{\partial \tilde{x}} \right) - h^2 \frac{\mathrm{d}R}{\mathrm{d}\tilde{h}} \frac{\partial \tilde{U}}{\partial \tilde{x}} = O(\varepsilon^{2+2\gamma}). \tag{52}$$

The expression (49) of R yields $R + \tilde{h}\mathrm{d}R/\mathrm{d}\tilde{h} = \mathrm{e}^{M^2}$ which leads to

$$\frac{\partial \tilde{h}}{\partial \tilde{t}} + \frac{\partial \tilde{h} \tilde{U}}{\partial \tilde{x}} = \frac{M^2}{2} Q_0 \tilde{h} \frac{\partial \tilde{U}}{\partial \tilde{x}} + O(\varepsilon^{2+2\gamma}) \tag{53}$$

where

$$Q_0 = \frac{2}{M^4} \left(\mathrm{e}^{-M^2} + M^2 - 1 \right). \tag{54}$$

The expression of Q_0 can also be written

$$Q_0 = 1 - \frac{M^2}{3} + O(M^4). \tag{55}$$

The fluid compressibility implies that the right-hand side of (53) is not zero. However the mass conservation equation is expressed by (51). Note that the exact depth-averaged mass conservation equation is

$$\frac{\partial h \overline{\rho}}{\partial t} + \frac{\partial h \overline{\rho} U}{\partial x} = 0 \tag{56}$$

and $\overline{\rho}/\rho_s = R + O(\varepsilon^{2+2\gamma})$.

2.3.3 Momentum balance equation

The integration of the momentum balance equation (44) in the horizontal direction, taking into account the boundary conditions, leads to

$$\frac{\partial \tilde{h} R \tilde{U}}{\partial \tilde{t}} + \frac{\partial}{\partial \tilde{x}} \left(\tilde{h} R \langle \tilde{u}^2 \rangle + \frac{1}{F^2} \int_0^{\tilde{h}} \tilde{p}_H \, \mathrm{d}\tilde{z} + \varepsilon^2 \tilde{h} \tilde{P} \right) = O(\varepsilon^{2+2\gamma}). \tag{57}$$

The definition of u' enables to write $\langle \tilde{u}^2 \rangle = \tilde{U}^2 + \varepsilon^{2\beta} \langle u'^2 \rangle$. Since $2\beta > 2$, the term of $O(\varepsilon^{2\beta})$ is negligible. The integral of the hydrostatic pressure can be calculated with the expression (19) which becomes in dimensionless form $M_0^2 \tilde{p}_H = \exp[M_0^2(\tilde{h} - \tilde{z})] - 1$. The depth-integrated horizontal momentum balance equation can be written

$$\frac{\partial \tilde{h} R \tilde{U}}{\partial \tilde{t}} + \frac{\partial}{\partial \tilde{x}} \left(\tilde{h} R \tilde{U}^2 + Q_1 \frac{\tilde{h}^2}{2F^2} + \varepsilon^2 \tilde{h} \tilde{P} \right) = O(\varepsilon^{2\beta}) + O(\varepsilon^{2+2\gamma}) \tag{58}$$

where

$$Q_1 = \frac{2}{M^4} \left(\mathrm{e}^{M^2} - M^2 - 1 \right) \tag{59}$$

which can be written

$$Q_1 = 1 + \frac{M^2}{3} + O(M^4). \tag{60}$$

In the vertical direction the integration over the depth of (40) with the boundary conditions gives

$$\frac{\partial \tilde{h} R \tilde{W}}{\partial \tilde{t}} + \frac{\partial \tilde{h} R \langle \tilde{u} \tilde{w} \rangle}{\partial \tilde{x}} = \tilde{p}_N(0) + O(\varepsilon^{2\gamma}) \tag{61}$$

where $\tilde{p}_N(0)$ is the value of the non-hydrostatic pressure at the bottom ($z = 0$). Since $\tilde{u} = \tilde{U} + \varepsilon^\beta \tilde{u}'$, we can write $\langle \tilde{u} \tilde{w} \rangle = \tilde{U} \tilde{W} + O(\varepsilon^\beta)$. An asymptotic expression of p_N is needed to evaluate $\tilde{p}_N(0)$.

Firstly, an asymptotic expression of the vertical velocity is obtained from the mass conservation equation (43) and from the decomposition $\tilde{u} = \tilde{U} + \varepsilon^\beta \tilde{u}'$:

$$\frac{\partial \tilde{w}}{\partial \tilde{z}} = -\frac{\partial \tilde{U}}{\partial \tilde{x}} + O(\varepsilon^\beta) + O(\varepsilon^{2\gamma}). \tag{62}$$

The integration of this relation with the no-penetration boundary condition shows that the variation of the vertical velocity in the depth is linear at this level of approximation. This gives

$$\tilde{w} = -\tilde{z} \frac{\partial \tilde{U}}{\partial \tilde{x}} + O(\varepsilon^\beta) + O(\varepsilon^{2\gamma}) \; ; \quad \tilde{W} = -\frac{\tilde{h}}{2} \frac{\partial \tilde{U}}{\partial \tilde{x}} + O(\varepsilon^\beta) + O(\varepsilon^{2\gamma}). \tag{63}$$

Secondly the non-hydrostatic pressure is obtained by the integration of the momentum balance equation in the vertical direction (40) which can be also consistently written

$$\frac{\partial \tilde{p}_N}{\partial \tilde{z}} = -\left(\frac{\partial \tilde{w}}{\partial \tilde{t}} + \frac{\partial \tilde{U} \tilde{w}}{\partial \tilde{x}} + \frac{\partial \tilde{w}^2}{\partial \tilde{z}} \right) + O(\varepsilon^\beta) + O(\varepsilon^{2\gamma}). \tag{64}$$

In this expression $\tilde{w}$ is replaced by the linear asymptotic law (63). The obtained relation is integrated from the free surface to an altitude z. At the free surface $z = h$ and the dynamic boundary condition gives $p_N(h) = 0$. It follows that the non-hydrostatic pressure profile in the depth is parabolic with

$$p_{\tilde{N}} = \frac{\tilde{h}^2 - \tilde{z^2}}{2} \left[2 \left(\frac{\partial \tilde{U}}{\partial \tilde{x}} \right)^2 - \frac{\partial^2 \tilde{U}}{\partial \tilde{x} \partial \tilde{t}} - \frac{\partial}{\partial \tilde{x}} \left(\tilde{U} \frac{\partial \tilde{U}}{\partial \tilde{x}} \right) \right] + O(\varepsilon^\beta) + O(\varepsilon^{2\gamma}). \tag{65}$$

Taking the usual depth average of (65) gives the average non-hydrostatic pressure $\tilde{P} = \overline{\tilde{p}_N}$

$$\tilde{P} = \frac{\tilde{h}^2}{3}\left[2\left(\frac{\partial \tilde{U}}{\partial \tilde{x}}\right)^2 - \frac{\partial^2 \tilde{U}}{\partial \tilde{x}\partial \tilde{t}} - \frac{\partial}{\partial \tilde{x}}\left(\tilde{U}\frac{\partial \tilde{U}}{\partial \tilde{x}}\right)\right] + O(\varepsilon^{\beta}) + O(\varepsilon^{2\gamma}). \tag{66}$$

This implies that

$$\tilde{p}_N(0) = \frac{3}{2}\tilde{P} + O(\varepsilon^{\beta}) + O(\varepsilon^{2\gamma}). \tag{67}$$

Consequently the depth-integrated vertical momentum balance equation is

$$\frac{\partial \tilde{h}R\tilde{W}}{\partial \tilde{t}} + \frac{\partial \tilde{h}R\tilde{U}\tilde{W}}{\partial \tilde{x}} = \frac{3}{2}\tilde{P} + O(\varepsilon^{\beta}) + O(\varepsilon^{2\gamma}). \tag{68}$$

2.3.4 Energy equation and non-hydrostatic pressure equation

So far four variables have been introduced to describe the depth-averaged flow: h, U, W and P. The average density R is not an independent variable since it is a function of h. Only three equations have been derived: (51), (58) and (68). The equation (53) is equivalent to (51). An evolution equation for P is needed to close the system.

The energy conservation equation (9) is integrated over the depth. With the decomposition of the density $\rho = \rho_H + \rho_N$, the integral of the sum of the internal energy and the potential energy is

$$\int_0^h (E_i + \rho_H g z + \rho_N g z)\,\mathrm{d}z = Q_2\frac{gh^2}{2} + \frac{gh^2 P}{a^2} + \frac{3}{5}Q_3\frac{hP^2}{a^2} \tag{69}$$

where

$$Q_2 = \frac{2}{M^4}\left[1 + \left(M^2 - 1\right)\mathrm{e}^{M^2}\right] \tag{70}$$

and $Q_3 = 1 + O(M^2)$. We can develop Q_2 as

$$Q_2 = 1 + \frac{2M^2}{3} + O(M^4). \tag{71}$$

In the right-hand side of (69) the second term corresponds to the non-hydrostatic perturbation to the density which is neglected in all equations of the model, being of $O(\varepsilon^{2+2\gamma})$. It is produced by the non-hydrostatic contribution to the potential energy $\rho_N g z$ and by the first-order term in ρ_N in the development (26) of the internal energy. In the scaling used to derive the model these terms are negligible. On the other hand the third term in the right-hand side of (69) is the analogue of an acoustic energy and plays the role of the internal energy of the model. This term leads to the evolution equation for the average non-hydrostatic pressure P. The term of $O(M^2)$ in Q_3 gives terms of $O(\varepsilon^{2\gamma})$ in the equation of P, which is already a quantity of $O(\varepsilon^2)$. As terms of $O(\varepsilon^{2+2\gamma})$ are negligible in this model, a consistent approximation is $Q_3 = 1$. It is possible to replace consistently Q_3 by R since $R = 1 + O(M^2)$ and consequently $Q_3 = R + O(M^2)$. The reason of this choice is that it leads to a model with a better mathematical structure while being still consistent. The factor $3/5$ is due to the shape factor of the parabolic distribution of the non-hydrostatic pressure in the fluid depth, which is thereafter denoted by r^2 with $r^2 = 6/5$.

In the flux of (9), the quantity $E_{iH} + \rho_H g z + p_H$ is equal to $\rho_H g h$. It follows that, to integrate over the depth the energy equation (9), we have to calculate the integral

$$\int_0^h \rho_H g h u\,\mathrm{d}z = ghU\int_0^h \rho_H\,\mathrm{d}z + gh\int_0^h \rho_H u'\,\mathrm{d}z, \tag{72}$$

taking into account the decomposition $u = U + u'$. In the right-hand side of this equation, the first integral is equal to hR and the second integral is equal to zero since by definition $\langle u' \rangle = 0$.

Consequently the integral of the energy equation (9) can be written

$$\frac{\partial}{\partial t}\left(hR\frac{\langle u^2\rangle}{2}+hR\frac{\langle w^2\rangle}{2}+Q_2\frac{gh^2}{2}+r^2\frac{hRP^2}{2a^2}\right) + \frac{\partial}{\partial x}\left[hR\frac{\langle u^3\rangle}{2}+hR\frac{\langle uw^2\rangle}{2}+r^2\frac{hRP^2}{2a^2}+gh^2RU+hUP\right]=0 \quad (73)$$

Neglecting terms of $O(\varepsilon^{2\beta})$, we can write $\langle u^2\rangle \simeq U^2$ and $\langle u^3\rangle \simeq U^3$. The term $\langle uw^2\rangle$ corresponds to terms of $O(\varepsilon^2)$ in the momentum balance equations. It is thus consistent to neglect the correction of $O(\varepsilon^\beta)$ writing $\langle uw^2\rangle \simeq U\langle w^2\rangle$. The linear profile of the vertical velocity (63) implies that

$$\langle w^2\rangle = \frac{4}{3}W^2. \quad (74)$$

It is also possible to define the deviation w' of w to its average value W as $w = W + w'$. With the expressions (63) of w and W, it is easy to calculate that $\langle w'^2\rangle = W^2/3$ giving $\langle w^2\rangle = W^2 + \langle w'^2\rangle = 4W^2/3$, since by definition $\langle w'\rangle = 0$.

In the energy, the term $Q_2gh^2/2$ is a potential energy. The momentum balance equation (58) can be written in dimensional form

$$\frac{\partial hRU}{\partial t}+\frac{\partial}{\partial x}\left(hRU^2+\Pi\right)=0 \quad (75)$$

where Π plays for the model the role of a pressure, with

$$\Pi = Q_1\frac{gh^2}{2}+hP. \quad (76)$$

Noticing that $Q_1 + Q_2 = 2R$, the energy conservation equation can be written

$$\frac{\partial hRe}{\partial t}+\frac{\partial}{\partial x}\left(hRUe+\Pi U\right)=0 \quad (77)$$

with the total energy

$$e = \frac{U^2}{2}+\frac{2W^2}{3}+\frac{Q_2}{R}\frac{gh}{2}+r^2\frac{P^2}{2a^2}. \quad (78)$$

From the depth-averaged mass and momentum equations (51), (75) and (68), it is possible to derive a balance equation for the mechanical energy of the model. Taking into account the mass conservation equation (51), the equations (75) and (68) can be written respectively

$$hR\left(\frac{\partial U}{\partial t}+U\frac{\partial U}{\partial x}\right)+\frac{\partial}{\partial x}\left(Q_1\frac{gh^2}{2}+hP\right)=0 \quad (79)$$

and

$$hR\left(\frac{\partial W}{\partial t}+U\frac{\partial W}{\partial x}\right)=\frac{3}{2}P. \quad (80)$$

Forming

$$\frac{1}{2}\left[U\times(75)+U\times(79)\right]+\frac{2}{3}\left[W\times(68)+W\times(80)\right] \quad (81)$$

and noticing that

$$U\frac{\partial}{\partial x}\left(Q_1\frac{gh^2}{2}\right)=\frac{\partial}{\partial t}\left(Q_2\frac{gh^2}{2}\right)+\frac{\partial}{\partial x}\left(gh^2RU\right), \quad (82)$$

we can obtain the depth-averaged mechanical energy balance equation

$$\frac{\partial hRe_M}{\partial t}+\frac{\partial}{\partial x}\left(hRUe_M+\Pi U\right)=\mathcal{P}_{\text{int}} \quad (83)$$

where the mechanical energy writes

$$e_M = \frac{U^2}{2} + \frac{2W^2}{3} + \frac{Q_2}{R}\frac{gh}{2} \tag{84}$$

and where the power of internal forces is

$$\mathcal{P}_{\text{int}} = P\left(2W + h\frac{\partial U}{\partial x}\right). \tag{85}$$

The power of internal forces is exchanged between the mechanical energy and the internal energy of the system. The difference between the total energy conservation equation (77) and the mechanical energy balance equation (83) gives the depth-averaged internal energy balance equation

$$\frac{\partial hRe_{\text{int}}}{\partial t} + \frac{\partial hRUe_{\text{int}}}{\partial x} = -\mathcal{P}_{\text{int}} \tag{86}$$

where the internal energy is

$$e_{\text{int}} = r^2\frac{P^2}{2a^2}. \tag{87}$$

The mass conservation equation (51) enables to write the internal energy equation (86) as

$$hR\frac{\mathrm{D}e_{\text{int}}}{\mathrm{D}t} = -\mathcal{P}_{\text{int}} \tag{88}$$

where the material derivative is defined as $\mathrm{D}/\mathrm{D}t = \partial/\partial t + U\partial/\partial x$. Deriving the expression (87) and using once more the mass conservation (51) yields the evolution equation of the average non-hydrostatic pressure

$$\frac{\partial hRP}{\partial t} + \frac{\partial hRUP}{\partial x} = -\frac{a^2}{r^2}\left(2W + h\frac{\partial U}{\partial x}\right). \tag{89}$$

This equation is a transport equation for the average non-hydrostatic pressure with a relaxation term on the average vertical velocity W.

2.3.5 Final system of equations

In dimensional form the final system of equations is

$$\frac{\partial h}{\partial t} + \frac{\partial hU}{\partial x} = \frac{M^2}{2}Q_0 h\frac{\partial U}{\partial x}, \tag{90}$$

$$\frac{\partial hRU}{\partial t} + \frac{\partial}{\partial x}\left(hRU^2 + Q_1\frac{gh^2}{2} + hP\right) = 0, \tag{91}$$

$$\frac{\partial hRW}{\partial t} + \frac{\partial hRUW}{\partial x} = \frac{3}{2}P, \tag{92}$$

$$\frac{\partial hRP}{\partial t} + \frac{\partial hRUP}{\partial x} = -\frac{a^2}{r^2}\left(2W + h\frac{\partial U}{\partial x}\right) \tag{93}$$

with R given by (49), M by (29), Q_0 by (54), Q_1 by (59) and where $r = \sqrt{6/5}$. This system admits the mass conservation equation

$$\frac{\partial hR}{\partial t} + \frac{\partial hUR}{\partial x} = 0 \tag{94}$$

and the energy conservation equation (77).

In the case of a constant bottom, the model of Escalante *et al.* (2019) is a particular case of the present model when the Mach number $M = 0$ (or if $\gamma > 1$), which implies that $R = Q_0 = Q_1 = 1$. The celerity c of Escalante *et al.* (2019) corresponds to a/r and their constant γ in the right-hand side of (92) is $3/2$ which is the only consistent value in this scaling. The model of Escalante *et al.* (2019) implies that the divergence of the velocity field is zero which leads to the usual average mass conservation equation

$$\frac{\partial h}{\partial t} + \frac{\partial hU}{\partial x} = 0. \tag{95}$$

The density is constant and the compressibility is felt indirectly, through the non-hydrostatic pressure. In this particular case, the Mach number is small enough to be able to neglect all density variations while the non-hydrostatic pressure is not negligible. As $\operatorname{div} \boldsymbol{v} \simeq 0$, this can be called the quasi-incompressible case. The motivation of this quasi-incompressible model is to obtain a hyperbolic approximation of the incompressible non-hydrostatic depth-averaged models in order to implement more efficient numerical schemes, as in Favrie & Gavrilyuk (2017).

By contrast, in the present model $\operatorname{div} \boldsymbol{v} \neq 0$ and the density is variable due to the hydrostatic corrections caused by depth variations. Since real compressible effects can be captured by the model, this case is really a compressible case, even if it is a weakly compressible case. It is not an approximation of the incompressible non-hydrostatic depth-averaged model even if the hyperbolicity is here too a desirable quality for the numerical resolution. These compressible effects are noticeable only for tsunamis in deep water where the Mach number M is in the 0.1–0.2 range. For coastal waves, the Mach number is smaller than 10^{-2} ($M^2 \sim 10^{-5}$) and the quasi-incompressible case is sufficient.

2.4 Hyperbolicity

The system (90)–(93) can be written in the form

$$\frac{\partial \overline{\mathbf{V}}}{\partial t} + \overline{\overline{\mathbf{A}}}\, \frac{\partial \overline{\mathbf{V}}}{\partial x} = \overline{\mathbf{S}} \tag{96}$$

where $\overline{\mathbf{V}} = (h, U, W, P)^{\mathrm{T}}$, $\overline{\mathbf{S}} = (0, 0, 3P/(2hR), -2a^2W/(r^2hR))^{\mathrm{T}}$ and

$$\overline{\overline{\mathbf{A}}} = \begin{bmatrix} U & \mathrm{e}^{-M^2}hR & 0 & 0 \\ g + P/(hR) & U & 0 & 1/R \\ 0 & 0 & U & 0 \\ 0 & a^2/(r^2R) & 0 & U \end{bmatrix}. \tag{97}$$

The four eigenvalues λ_1, λ_2, λ_3 and λ_4 of this matrix are the characteristics of the system which are

$$\lambda_{1,2} = U \; ; \quad \lambda_{3,4} = U \pm \sqrt{\mathrm{e}^{-M^2}\,(ghR + P) + \frac{a^2}{r^2R^2}}. \tag{98}$$

Since P is very small and a is large, these characteristics are real. Furthermore it is possible to find four linearly independent eigenvectors. The system is thus hyperbolic.

In the celerity $\sqrt{\mathrm{e}^{-M^2}\,(ghR + P) + a^2/(r^2R^2)}$, the largest term by far is due to the sound velocity $a^2/(r^2R^2)$. The average density R is slightly larger than 1 and $r = \sqrt{6/5}$. The effect of these factors, mainly r, is to decrease slightly the effective sound velocity which is $a_{\mathrm{eff}} = a/(rR)$ (note that this has no effect on the Mach number M which depends on a but not on r). If the model is used for coastal waves, where the compressible effects are completely negligible, then an artificial value of r, much larger than 1, can be used to decrease the effective sound velocity and consequently to increase the time step, which reduces the computational time. This is equivalent to adding an artificial compressibility to the system in the same manner as in the

pseudo-compressible approach of Auclair *et al.* (2018). In the nearshore region, values of r as high as 10–50 can be used giving an effective sound velocity of the same order of magnitude as the celerities used in Favrie & Gavrilyuk (2017) and Escalante *et al.* (2019). For tsunamis in deep oceans, the physical value of r should be kept.

2.5 Dispersive properties

The linear dispersive properties of the model are studied from the derivation of the dispersion relation for the system of equations (90)–(93). These equations are linearized around the equilibrium state h_0, $R_0 = [\exp(M_0^2) - 1]/M_0^2$, $U_0 = 0$, $W_0 = 0$ and $P_0 = 0$ considering small perturbations h', U', W' and P':

$$h = h_0 + h' \; ; \quad U = U' \; ; \quad W = W' \; ; \quad P = P'. \tag{99}$$

The linearized equations can be written

$$\frac{\partial h'}{\partial t} + \mathrm{e}^{-M_0^2} h_0 R_0 \frac{\partial U'}{\partial x} = 0, \tag{100}$$

$$\frac{\partial U'}{\partial t} + g\frac{\partial h'}{\partial x} + \frac{1}{R_0}\frac{\partial P'}{\partial x} = 0, \tag{101}$$

$$\frac{\partial W'}{\partial t} = \frac{3}{2}\frac{P'}{h_0 R_0}, \tag{102}$$

$$\frac{\partial P'}{\partial t} + \frac{a^2}{r^2 R_0^2}\frac{\partial U'}{\partial x} = -\frac{2a^2 W'}{r^2 h_0 R_0}. \tag{103}$$

These perturbations are taken of the form

$$\left[h', U', W', P'\right]^{\mathrm{T}} = [A_1, A_2, A_3, A_4]^{\mathrm{T}} \, \mathrm{e}^{\mathrm{i}(kx - \omega t)}. \tag{104}$$

This leads to the dispersion relation

$$\frac{r^2 h_0^2 R_0^2}{3a^2}\omega^4 - \omega^2 \left[1 + \frac{k^2 h_0^2}{3}\left(1 + r^2 M_0^2 \mathrm{e}^{-M_0^2} R_0^3\right)\right] + \mathrm{e}^{-M_0^2} k^2 g h_0 R_0 = 0. \tag{105}$$

In dimensionless form, for low frequencies $\varepsilon\tilde{\omega} = \omega\sqrt{h_0/g}$ and with the longwave scaling $\varepsilon\tilde{k} = kh_0$, the dispersion relation is

$$\tilde{\omega}^2 \left(1 + \varepsilon^2 \frac{\tilde{k}^2}{3}\right) = \mathrm{e}^{-M_0^2} R_0 \tilde{k}^2 + O(\varepsilon^{2+2\gamma}). \tag{106}$$

If $2\gamma = 2$, $M_0^2 = \varepsilon^2 M_1^2$, then, at the order $O(1)$, the dispersion relation reduces to $\tilde{\omega}^2 = \tilde{k}^2$ giving the phase velocity of the incompressible Saint-Venant equations $v_\varphi = \sqrt{gh_0}$. At the following order $O(\varepsilon^2)$, the dispersion relation can be developed into

$$\tilde{\omega}^2 = \tilde{k}^2 \left(1 - \varepsilon^2 \frac{M_1^2}{2} - \varepsilon^2 \frac{\tilde{k}^2}{3}\right) + O(\varepsilon^4). \tag{107}$$

If $2\gamma = 1$, $M_0^2 = \varepsilon M_1^2$, then the dispersion relation reduces at order $O(\varepsilon)$ to

$$\tilde{\omega}^2 = \tilde{k}^2 \mathrm{e}^{-M_0^2} R_0, \tag{108}$$

which can be written

$$\tilde{\omega}^2 = \tilde{k}^2 \left(1 - \varepsilon \frac{M_1^2}{2}\right) + O(\varepsilon^2). \tag{109}$$

At the following order, the dispersion relation is

$$\tilde{\omega}^2 = \tilde{k}^2 \left(1 - \varepsilon \frac{M_1^2}{2} + \varepsilon^2 \frac{M_1^4}{6} - \varepsilon^2 \frac{\tilde{k}^2}{3} \right) + O(\varepsilon^3). \tag{110}$$

All these expresions show that, even at the longwave limit, the dispersion relation is modified by compressibility effects. The phase velocity for $k \to 0$ is thus

$$v_\varphi = \sqrt{g h_0 \mathrm{e}^{-M_0^2} R_0} \tag{111}$$

which is practically

$$v_\varphi \simeq \sqrt{g h_0} \left(1 - \frac{M_0^2}{4} \right), \tag{112}$$

for $2\gamma = 2$, and

$$v_\varphi \simeq \sqrt{g h_0} \left(1 - \frac{M_0^2}{4} + \frac{5 M_0^4}{96} \right), \tag{113}$$

for $2\gamma = 1$. Compared to the incompressible case, the phase velocity is slightly smaller due to the compressibility of water. For typical ocean depths, this diminution of the phase velocity is of the order of 0.5 %.

The dispersion relation in the linear theory of compressible fluids is (Pidduck 1910, Dalrymple & Roger 2007, Kadri 2015, Abdolali & Kirby 2017)

$$\omega^2 = g \frac{\left(\kappa^2 - \Gamma^2 \right) \tanh(\kappa h_0)}{\kappa - \Gamma \tanh(\kappa h_0)} \tag{114}$$

where $\Gamma = g/(2a^2)$ and $\kappa = \sqrt{k^2 - \omega^2/a^2 + \Gamma^2}$. Using the same low frequency and longwave scaling as above (the low frequency scaling eliminating the acoustic modes) and $M_0 = O(\varepsilon^{2\gamma})$, this dispersion relation gives exactly the same relation dispersion as the model: If $2\gamma = 2$, (114) gives (107) and if $2\gamma = 1$, (114) gives (110). At the limit $\gamma \to 0$, which is the longwave limit where the compressible effects are much larger than the dispersive effects, the dispersion relation (114) of the linear theory reduces to

$$\tilde{\omega}^2 = \frac{\left(\tilde{k}^2 - \varepsilon^{2\gamma} M_1^2 \tilde{\omega}^2 \right) \tanh\left(\varepsilon^{2\gamma} M_1^2 / 2 \right)}{\left(\varepsilon^{2\gamma} M_1^2 / 2 \right) \left(1 - \tanh\left(\varepsilon^{2\gamma} M_1^2 / 2 \right) \right)} + O(\varepsilon^2) \tag{115}$$

The solution of this equation can be written

$$\tilde{\omega}^2 = \tilde{k}^2 \mathrm{e}^{-M_0^2} R_0 + O(\varepsilon^2) \tag{116}$$

which is the same expression as given by the model for the same scaling and the same limit. It follows that the phase velocity at the longwave limit with compressible effects is the same in the model and in the linear theory and its expression is (111). This is also the expression of the group velocity since, at this limit, there is no dispersion. In the development of (111)

$$\frac{v_\varphi}{\sqrt{g h_0}} = 1 - \frac{M_0^2}{4} + \frac{5}{96} M_0^4 - \frac{M_0^6}{128} + \frac{79}{92160} M_0^8 + O(M_0^{10}), \tag{117}$$

only terms of order n in M_0^2 with $n = 1/\gamma$ have a meaning since the first dispersive term is $O(\varepsilon^2)$. This implies that, in practice, the expressions (112) or (113) are sufficient and consistent. The variation of the dimensionless phase velocity $v_\varphi/\sqrt{g h_0}$ with the depth is shown in Figure 1. This variation is almost linear with h_0 since it is given with a good approximation by (112) which

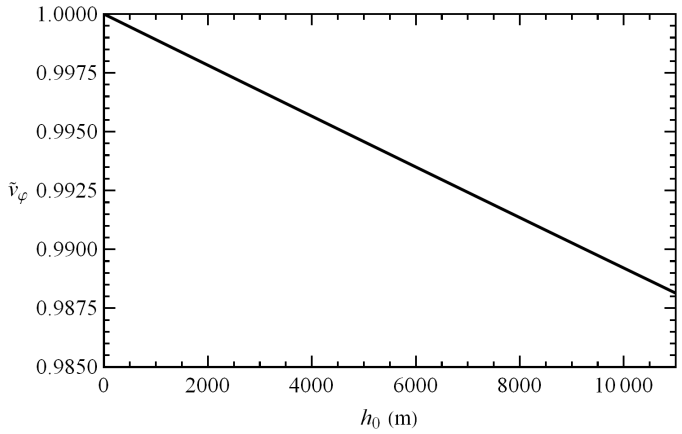

Figure 1: Dimensionless phase velocity $v_\varphi/\sqrt{gh_0}$ as a function of the depth h_0.

gives $\tilde{v}_\varphi \simeq 1 - gh_0/(4a^2)$. In most cases the relative diminution of the phase velocity due to compressibility is smaller than 1 %.

The model is thus fully consistent with the general linear theory of compressible fluids with respect to compressible effects at the longwave limit. It is also consistent to the first order in k^2 for dispersive effects in the same way as the incompressible Serre-Green-Naghdi model.

The complete dispersion relation (105) can be explicitly solved. The solutions of this equation divide into a slow branch and a fast branch. Their expressions are given by

$$\tilde{\omega}^2 = \frac{1}{2r^2M_0^2R_0^2}\left[3 + \tilde{k}^2\left(1 + r^2M_0^2R_0^3\mathrm{e}^{-M_0^2}\right) \pm\sqrt{\left(3+\tilde{k}^2\right)^2 + 2r^2M_0^2R_0^3\mathrm{e}^{-M_0^2}\tilde{k}^2\left(\tilde{k}^2-3\right) + r^4M_0^4R_0^6\mathrm{e}^{-2M_0^2}\tilde{k}^4}\right] \quad (118)$$

with the minus sign for the slow branch and the plus sign for the fast branch. Since the fast branch corresponds to an acoustic mode and the slow branch to the usual solution in hydraulics of free surface flows but for the compressible corrections, they will be also called thereafter the acoustic branch and the hydraulic branch respectively. These solutions are presented in Figure 2 for $h_0 = 6000\,\mathrm{m}$ with the angular frequency and the phase velocity of both branches as a function of $\tilde{k}$ in Figure 2 (a) and (b) respectively. The acoustic branch has a cutoff frequency $\tilde{\omega}_c = \sqrt{3}/(rM_0R_0)$ or, in dimensional form,

$$\omega_c = \frac{a\sqrt{3}}{rR_0h_0} \quad (119)$$

which is the angular frequency of the fast branch at $k = 0$. There is no acoustic mode at a lower frequency. The phase velocity of the acoustic mode, denoted by v_φ^a, can be written

$$\tilde{v}_\varphi^a = \frac{1}{rM_0R_0}\sqrt{1+\frac{3}{\tilde{k}^2}} + O(M_0)\,; \quad v_\varphi^a \simeq \frac{a}{rR_0}\sqrt{1+\frac{3}{k^2h_0^2}}. \quad (120)$$

This velocity is infinite when $M_0 = 0$ (or $a \to \infty$), which is the incompressible limit, and decreases monotonously when the Mach number, or the wave number, increases. In practice, the value of the acoustic phase velocity is slightly higher than the value given by the above expression, due to the corrective term of $O(M_0)$. For $k \to \infty$, the acoustic phase velocity is almost equal to the effective sound velocity

$$a_{\mathrm{eff}} = \frac{a}{rR_0}. \quad (121)$$

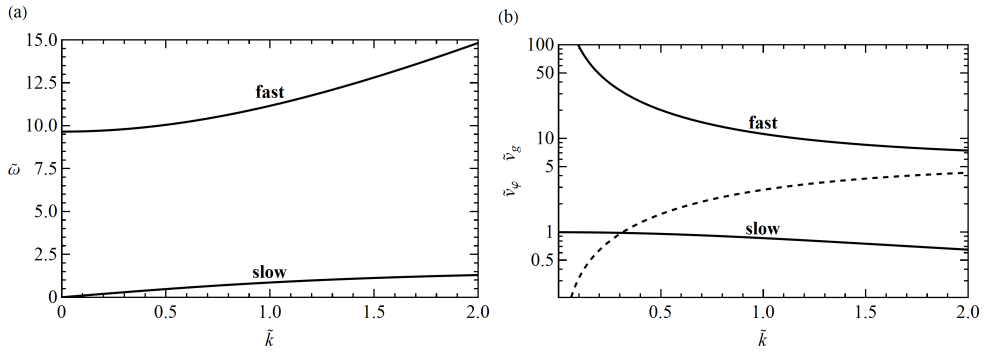

Figure 2: Solutions of the relation dispersion with the fast or acoustic branch and the slow or hydraulic branch for $h_0 = 6000\,\mathrm{m}$: (a) angular frequency and (b) phase velocity. The dashed curve in (b) is the group velocity of the acoustic branch.

In fact, the high wave number limit is slightly larger than this value. This implies that the phase velocity of the acoustic mode, if it exists, is larger than the effective sound velocity and, for sufficiently low wave numbers, much larger than the sound velocity. It is of course the opposite for the group velocity of the acoustic mode which is equal to 0 for $k = 0$ and which is smaller than the sound velocity (see the dashed curve in Figure 2).

In the power series expansion of the phase velocity of the slow branch, the factor r appears only at the order $O(\tilde{k}^4 M_0^2) = O(\varepsilon^{4+2\gamma})$. It has no influence on the longwave limit and its compressible correction nor on the leading dispersive term of $O(\tilde{k}^2)$. This means that the factor r has a very small influence on the hydraulic properties (depending on the slow branch). On the contrary, r appears in the leading term of the acoustic branch. A value of r larger than 1 decreases the effective sound velocity and the characteristics of the system (see (98)) which enables to increase the time step in the numerical resolution. It is thus possible to choose an artificially higher value of r to decrease the computational time with no significant effect on the free-surface hydraulics properties, not even on the compressible corrections which depend on the Mach number but not on r. This possibility is similar to the method, used by several authors (Auclair *et al.* 2018, Escalante *et al.* 2019 for example), of adding an artificial compressibility to the system for a better numerical efficiency.

2.6 Equations with improved dispersive properties

Most earthquake-generated tsunamis have long wavelengths and thus small dispersive effects. However at long distances, dispersive effects are not negligible (Kirby *et al.* 2013). Furthermore tsunamis generated by submarine landslides have shorter wavelengths and consequently important dispersive effects even in the near field (Tappin *et al.* 2014). The model derived so far has accurate dispersive properties for long waves but these properties deteriorate quickly for shorter wavelengths and this deterioration is increased if the depth is larger due to more important compressible effects. As one of the purposes of this model is to capture a diminution of the phase velocity of only 0.5 % due to compressibility, a very high accuracy on the phase velocity and on the dispersive properties is needed, even for tsunamis with a relatively short wavelength. Most operational Boussinesq-type models include some method to improve the dispersive properties (see for example Nwogu 1993, Wei *et al.* 1995, Kennedy *et al.* 2001, Bonneton *et al.* 2011).

In this paper, the method of Bonneton *et al.* (2011) is adapted for this compressible model and for the specific case of tsunamis. However this is not sufficient as the improvement of the dispersive properties with this method alone depends heavily on the Mach number and thus is not satisfactory for all ocean depths. Consequently an additional correction is applied for the compressible effects.

Both corrections need to be consistent with respect to the asymptotic method used to derive the model. This means that the model with improve dispersive properties has to be asymptotically equivalent to the original model, differing only by terms of $O(\varepsilon^{2+2\gamma})$ or smaller.

The first idea is to use the vertical velocity at some height above the bottom as a variable instead of the average vertical velocity. More precisely the new variable W^* is defined as the value of w at a relative height $\alpha/2$ above the bottom with respect to the water depth i.e.

$$\frac{\alpha}{2} = \frac{z}{h}. \tag{122}$$

This coefficient α coincides with the coefficient of the method of Bonneton *et al.* (2011) but it has here a clear physical meaning. The definition

$$W^* = w|_{z=\alpha h/2}\,, \tag{123}$$

and the asymptotic expression of w (63) yields the asymptotic expression

$$\tilde{W}^* = -\frac{\alpha}{2}\tilde{h}\frac{\partial \tilde{U}}{\partial \tilde{x}} + O(\varepsilon^{\beta}) + O(\varepsilon^{2\gamma}) \tag{124}$$

which leads to

$$\tilde{W}^* = \tilde{W} + \frac{1-\alpha}{2}\tilde{h}\frac{\partial \tilde{U}}{\partial \tilde{x}} + O(\varepsilon^{\beta}) + O(\varepsilon^{2\gamma}). \tag{125}$$

Consequently an equation for W^* can be obtained from the equation of W as

$$\tilde{h}R\frac{\mathrm{D}\tilde{W}^*}{\mathrm{D}\tilde{t}} = \tilde{h}R\frac{\mathrm{D}\tilde{W}}{\mathrm{D}\tilde{t}} + \frac{\alpha-1}{2}\tilde{h}^2R\left[2Q_4\left(\frac{\partial \tilde{U}}{\partial \tilde{x}}\right)^2 - \frac{\partial}{\partial \tilde{x}}\left(\frac{\mathrm{D}\tilde{U}}{\mathrm{D}\tilde{t}}\right)\right] + O(\varepsilon^{\beta}) + O(\varepsilon^{2\gamma}) \tag{126}$$

where $Q_4 = [M^2 + 1 - \exp(-M^2)]/(2M^2) = 1 - M^2/4 + O(M^4)$. The key point of the approach of Bonneton *et al.* (2011) is to use an asymptotically equivalent set of equations by noting that

$$\tilde{h}R\frac{\mathrm{D}\tilde{U}}{\mathrm{D}\tilde{t}} = -\frac{\partial}{\partial \tilde{x}}\left(\frac{Q_1\tilde{h}^2}{2F^2}\right) + O(\varepsilon^2) + O(\varepsilon^{2\beta}). \tag{127}$$

Since the evolution equation of W is accurate to within terms of $O(\varepsilon^{2\gamma})$ or $O(\varepsilon^{\beta})$, we can write to the same approximation

$$\tilde{h}R\frac{\mathrm{D}\tilde{W}^*}{\mathrm{D}\tilde{t}} = \tilde{h}R\frac{\mathrm{D}\tilde{W}}{\mathrm{D}\tilde{t}} + \frac{\alpha-1}{2}\tilde{h}^2R\left[2Q_4\left(\frac{\partial \tilde{U}}{\partial \tilde{x}}\right)^2 + \frac{1}{F^2}\frac{\partial^2 \tilde{h}}{\partial \tilde{x}^2}\right] + O(\varepsilon^{\beta}) + O(\varepsilon^{2\gamma}). \tag{128}$$

Using (68) and reverting to dimensional quantities lead to

$$\frac{\partial hRW^*}{\partial t} + \frac{\partial hRUW^*}{\partial x} = \frac{3}{2}P + \frac{\alpha-1}{2}h^2R\left[2Q_4\left(\frac{\partial U}{\partial x}\right)^2 + g\frac{\partial^2 h}{\partial x^2}\right]. \tag{129}$$

Replacing W with its expression depending on W^* in (89) gives the evolution equation of the average non-hydrostatic pressure

$$\frac{\partial hRP}{\partial t} + \frac{\partial hRUP}{\partial x} = -\frac{a^2}{r^2}\left(2W^* + \alpha h\frac{\partial U}{\partial x}\right). \tag{130}$$

The other equations are not modified. The problem of the equation (129) is the presence of the second derivative $\partial^2 h/\partial x^2$. To preserve a well-posed hyperbolic structure for the model, a new variable S, directly related to the slope of the free surface, is defined as

$$S = \alpha\frac{\partial h}{\partial x}. \tag{131}$$

An evolution equation for S can be derived from the averaged mass conservation equation (90) which enables to write

$$\frac{\mathrm{D}}{\mathrm{D}t}\left(\frac{\partial h}{\partial x}\right) = -\frac{\partial}{\partial x}\left(\mathrm{e}^{-M^2} hR\frac{\partial U}{\partial x}\right) - \frac{\partial h}{\partial x}\frac{\partial U}{\partial x}. \tag{132}$$

Using the asymptotic expression of W^* (124) and the definition (131) of S, and neglecting terms of $O(\varepsilon^{2\gamma})$ in the equation of S since they would produce terms of $O(\varepsilon^{2+2\gamma})$ in the model, lead to the evolution equation of S

$$\frac{\partial hRS}{\partial t} + \frac{\partial hRUS}{\partial x} = 2h\frac{\partial W^*}{\partial x} + \frac{2W^*S}{\alpha}. \tag{133}$$

The evolution equation of W^* (129) can thus be written, neglecting again terms of $O(\varepsilon^{2\gamma})$ (for example $Q_4 = 1 + O[\varepsilon^{2\gamma}]$),

$$\frac{\partial hRW^*}{\partial t} + \frac{\partial hRUW^*}{\partial x} = \frac{3}{2}P + \frac{\alpha-1}{2\alpha}gh^2R\frac{\partial S}{\partial x} + 4\frac{\alpha-1}{\alpha^2}W^{*2}. \tag{134}$$

The complete model is composed of equations (90), (91), (134), (130) and (133). The dispersive properties are indeed improved but either they are still not accurate enough for tsunamis or the value of the coefficient α giving accurate properties depends on the Mach number and thus on the depth. A compressible correction is thus needed.

Since $R = 1 + O(\varepsilon^{2\gamma})$, a term in equations (134), (130) or (133), which are accurate to within terms of $O(\varepsilon^{2\gamma})$, can be multiplied by R without changing the accuracy of the model. The following model is thus consistent with the model (90)–(93)

$$\frac{\partial h}{\partial t} + \frac{\partial hU}{\partial x} = \frac{M^2}{2}Q_0 h\frac{\partial U}{\partial x}, \tag{135}$$

$$\frac{\partial hRU}{\partial t} + \frac{\partial}{\partial x}\left(hRU^2 + Q_1\frac{gh^2}{2} + hP\right) = 0, \tag{136}$$

$$\frac{\partial hRW^*}{\partial t} + \frac{\partial hRUW^*}{\partial x} = \frac{3}{2}R^2P + \frac{\alpha-1}{2\alpha}gh^2R\frac{\partial S}{\partial x} + 4\frac{\alpha-1}{\alpha^2}W^{*2}, \tag{137}$$

$$\frac{\partial hRP}{\partial t} + \frac{\partial hRUP}{\partial x} = -\frac{a^2}{r^2}\left(2R^2W^* + \alpha h\frac{\partial U}{\partial x}\right), \tag{138}$$

$$\frac{\partial hRS}{\partial t} + \frac{\partial hRUS}{\partial x} = \frac{2h}{R^3}\frac{\partial W^*}{\partial x} + \frac{2W^*S}{\alpha}. \tag{139}$$

This model satisfies exactly the mass conservation equation (94). If $\alpha = 1$, the system reduces to the four-equation model (135)–(138) since the fifth equation (139) is useless in this case. This system satisfies also exactly the energy conservation equation (77) with the same energy (78) and the same expression (76) of Π. The compressible correction, formed by the factor R^2 in the first term at the right-hand side of (137) and (138), preserves the exact conservation of energy. On the other hand, this is not the case for the other correction, due to the coefficient α. If $\alpha \neq 1$, the system has five equations and the energy conservation is not satisfied exactly but only asymptotically. This is the drawback of this method since there is the same problem in the incompressible case (see Bonneton *et al.* 2011).

The system (136)–(139) is a system of five equations which can be written in the form

$$\frac{\partial \overline{\mathbf{V}}^*}{\partial t} + \overline{\overline{\mathbf{A}}}^* \frac{\partial \overline{\mathbf{V}}^*}{\partial x} = \overline{\mathbf{S}}^* \tag{140}$$

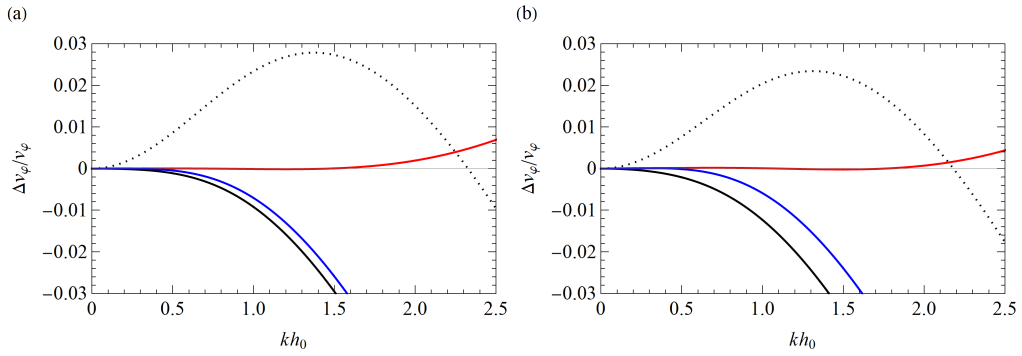

Figure 3: Relative deviation of the phase velocity with respect to the linear theory of compressible fluids for (a) $h_0 = 2000\,\mathrm{m}$ and (b) $h_0 = 6000\,\mathrm{m}$: Model with standard dispersive properties (black), model with improved dispersive properties and $\alpha = 1$ (blue), model with improved dispersive properties and $\alpha = 1.19$ (red) and model with the assumption of a linear profile for the non-hydrostatic pressure (dotted curve).

where $\overline{\mathbf{V}}^* = (h, U, W^*, P, S)^{\mathrm{T}}$,

$$\overline{\mathbf{S}}^* = \left(0, 0, \frac{3RP}{2h} + 4\frac{\alpha-1}{\alpha^2}\frac{W^{*2}}{hR}, -\frac{2a^2RW^*}{r^2h}, \frac{2W^*S}{\alpha hR}\right)^{\mathrm{T}}, \tag{141}$$

and

$$\overline{\overline{\mathbf{A}}}^* = \begin{bmatrix} U & \mathrm{e}^{-M^2}hR & 0 & 0 & 0 \\ g + P/(hR) & U & 0 & 1/R & 0 \\ 0 & 0 & U & 0 & -(\alpha-1)gh/(2\alpha) \\ 0 & \alpha a^2/(r^2R) & 0 & U & 0 \\ 0 & 0 & -2/R^4 & 0 & U \end{bmatrix}. \tag{142}$$

The five eigenvalues of this matrix are

$$\lambda_1 = U\ ; \quad \lambda_{2,3} = U \pm \frac{\sqrt{gh}}{R^2}\sqrt{\frac{\alpha-1}{\alpha}}\ ; \quad \lambda_{4,5} = U \pm \sqrt{(ghR+P)\,\mathrm{e}^{-M^2} + \frac{\alpha a^2}{r^2R^2}}. \tag{143}$$

The model is hyperbolic if $\alpha > 1$. Note that the value chosen by Bonneton *et al.* (2011) is $\alpha = 1.159$ and satisfies this condition.

The dispersive properties are studied with the same method as in §2.5 with $S = 0$ in the equilibrium state used for the linearization. Using the scaling $\tilde{\omega} = \omega\sqrt{h_0/g}$ and $\tilde{k} = kh_0$, the dispersion relation of system (135)–(139) is

$$\frac{r^2M_0^2}{3R_0^2}\tilde{\omega}^4 - \tilde{\omega}^2\left(1 + \alpha\frac{\tilde{k}^2}{3R_0^4} + \frac{M_0^2}{3}\frac{r^2\mathrm{e}^{-M_0^2}}{R_0}\tilde{k}^2 + \frac{\alpha-1}{\alpha}\frac{M_0^2}{3}\frac{r^2}{R_0^6}\tilde{k}^2\right) + \tilde{k}^2\left(R_0\mathrm{e}^{-M_0^2} + \frac{\alpha-1}{\alpha}\frac{M_0^2}{3}\frac{r^2\mathrm{e}^{-M_0^2}}{R_0^5}\tilde{k}^2 + \frac{\alpha-1}{3}\frac{\tilde{k}^2}{R_0^8}\right) = 0. \tag{144}$$

The value $\alpha = 1.159$ used by Bonneton *et al.* (2011) is appropriate for coastal waves. It gives accurate values of the phase velocity until $kh_0 \simeq 4$. However for tsunamis, the accuracy is not sufficient in the crucial range $0 \leqslant kh_0 \leqslant 1.5$. On the other hand, it is not necessary to keep a high accuracy until $kh_0 = 4$. Given that the compressibility entails a decrease of the phase velocity of about 0.5 %, a much higher accuracy is needed for the tsunamis wavelengths. The value which will be used thereafter is

$$\alpha = 1.19. \tag{145}$$

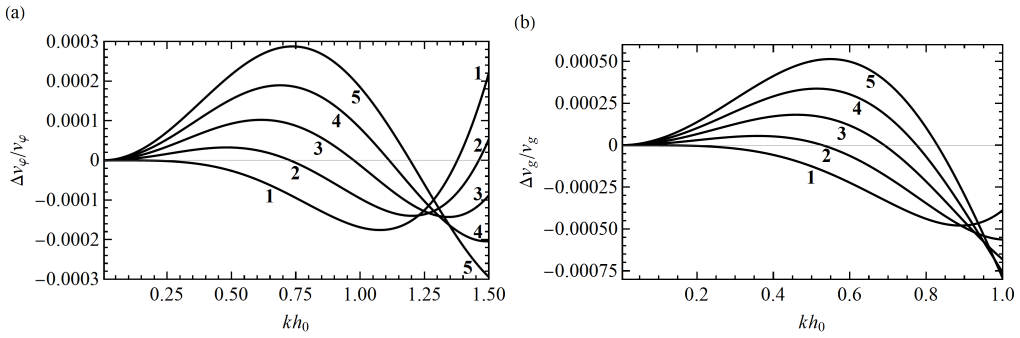

Figure 4: Relative deviation of the phase velocity (a) and of the group velocity (b) with respect to the linear theory of compressible fluids for $h_0 = 10\,\mathrm{m}$ (curve 1), $h_0 = 2000\,\mathrm{m}$ (curve 2), $h_0 = 4000\,\mathrm{m}$ (curve 3), $h_0 = 6000\,\mathrm{m}$ (curve 4) and $h_0 = 8000\,\mathrm{m}$ (curve 5).

This value is larger than 1 and the system is thus hyperbolic. The relative deviation of the phase velocity defined by $(v_\varphi - v_\varphi^{\mathrm{lin}})/v_\varphi^{\mathrm{lin}}$ where v_φ^{lin} is the phase velocity given by the linear theory of compressible fluids (with the dispersion relation (114)) is presented in Figure 3 for $h_0 = 2000\,\mathrm{m}$ (Figure 3 (a)) and for $h_0 = 6000\,\mathrm{m}$ (Figure 3 (b)). The black curve is the standard model (90)–(93), the blue curve is the energy-conserving model with improved dispersive properties and $\alpha = 1$ (i.e. the four equations (135)–(138) with $\alpha = 1$) and the red curve is the five-equation model (135)–(139) with improved dispersive properties and $\alpha = 1.19$.

The standard model gives an accurate value for small wavelengths but the deviation is already too large at $kh_0 = 0.5$. The extended model with improved dispersive properties gives a very accurate value of the phase velocity until at least $kh_0 = 0.5$ if $\alpha = 1$ and $kh_0 = 1.5$ if $\alpha = 1.19$. For $h_0 = 6000\,\mathrm{m}$, the relative error is smaller than 0.1 % if $kh_0 \leqslant 0.365$ for the standard model, if $kh_0 \leqslant 0.672$ for the four-equation modified model with $\alpha = 1$ and if $kh_0 \leqslant 2.06$ for the five-equation extended model with $\alpha = 1.19$. As can be seen on Figure 3 the relative error given by the extended model with $\alpha = 1.19$ on the phase velocity is very close to 0 for all depths if $kh_0 \leqslant 1.5$.

The relative deviation on the phase velocity given by the extended model (135)–(139) and $\alpha = 1.19$ is also presented in Figure 4 (a), for $h_0 = 10\,\mathrm{m}$ (an almost incompressible case), $h_0 = 2000\,\mathrm{m}$, $h_0 = 4000\,\mathrm{m}$, $h_0 = 6000\,\mathrm{m}$ and $h_0 = 8000\,\mathrm{m}$ in the range $0 \leqslant kh_0 \leqslant 1.5$. In this range, the relative deviation is always smaller than 0.03 % at all depths. The relative deviation on the group velocity for $0 \leqslant kh_0 \leqslant 1$ is presented in Figure 4 (b) for the same depths as above. In this range, this deviation on the group velocity is always smaller than 0.08 %. The phase velocity and the group velocity of the extended model are thus highly accurate for typical wavelengths of tsunamis for all depths which enables to capture the compressible effects on the propagation of tsunamis.

Some authors proposed an alternative incompressible model to the Serre-Green-Naghdi model by assuming that the depth profile of the non-hydrostatic pressure is linear instead of parabolic. This linear profile was implicitly used by Stelling & Zijlema (2003) without justification in order to approximate the integral over the depth of the non-hydrostatic pressure. A linear profile was also used by Walters (2005) to maintain compatibility with the numerical method. An incompressible model with such a linear profile was proposed by Bristeau *et al.* (2015) and a hyperbolic approximation was developed by Escalante *et al.* (2019). This assumption leads to a model which is not consistent with a longwave scaling, giving in particular a deviation to the dispersion relation of the linear theory of Airy at the first order in k. The approach used above to derive the standard model can be used with the artificial assumption of a linear vertical profile for the non-hydrostatic pressure. The only difference is that the factor 3/2 in (93) is replaced by

a factor 2. The relative deviation given by this approach on the phase velocity is presented in Figure 3 (dotted curve). The deviation is smaller than 0.1 % until $kh_0 = 0.169$ only instead of 0.365. Due to the inconsistency of this linear profile, the error increases more quickly than for the standard model when the wavelength increases and is of the order of 1 % in the wavelength range of tsunamis. This makes this approach unsuited to capture accurately the compressible effects on the propagation of tsunamis.

2.7 Acoustic subsystem

Splitting is a common strategy used for the numerical resolution of systems of nonlinear hyperbolic equations. A physical splitting is also interesting to get an insight about the different waves governed by a model as was shown by Gavrilyuk *et al.* (2018) for a 2D-model of sheared shallow water flows having two different families of waves besides contact characteristics. A splitting method applied to the present model (in its standard form) can divide the full system into a slow – or hydraulic – subsystem and a fast – or acoustic – subsystem. The hydraulic subsystem is

$$\frac{\partial h}{\partial t} + \frac{\partial hU}{\partial x} = \frac{M^2}{2} Q_0 h \frac{\partial U}{\partial x}, \tag{146}$$

$$\frac{\partial hRU}{\partial t} + \frac{\partial}{\partial x}\left(hRU^2 + Q_1 \frac{gh^2}{2} \right) = 0, \tag{147}$$

$$\frac{\partial hRW}{\partial t} + \frac{\partial hRUW}{\partial x} = 0, \tag{148}$$

$$\frac{\partial hRP}{\partial t} + \frac{\partial hRUP}{\partial x} = 0. \tag{149}$$

This subsystem can also be written

$$\frac{\partial \overline{\mathbf{V}}}{\partial t} + \overline{\overline{\mathbf{A}}}_{\mathbf{H}} \frac{\partial \overline{\mathbf{V}}}{\partial x} = 0 \tag{150}$$

where

$$\overline{\overline{\mathbf{A}}}_{\mathbf{H}} = \begin{bmatrix} U & \mathrm{e}^{-M^2} hR & 0 & 0 \\ g & U & 0 & 0 \\ 0 & 0 & U & 0 \\ 0 & 0 & 0 & U \end{bmatrix}. \tag{151}$$

The four eigenvalues of this matrix are $\lambda_{1,2} = U$ and $\lambda_{3,4} = U \pm \sqrt{\mathrm{e}^{-M^2} ghR}$. There is four linearly independent eigenvectors and the system is hyperbolic. In the incompressible limit, where $M = 0$ and $R = 1$, this system reduces to the classical Saint-Venant equations (or nonlinear shallow water equations) with two additional transport equations for W and P, hence the name "hydraulic" of this subsystem, with the well-known characteristics $U \pm \sqrt{gh}$. The compressibility adds only some compressible corrections.

The acoustic subsystem writes

$$\frac{\partial h}{\partial t} = 0, \tag{152}$$

$$\frac{\partial hRU}{\partial t} + \frac{\partial hP}{\partial x} = 0, \tag{153}$$

$$\frac{\partial hRW}{\partial t} = \frac{3}{2} P, \tag{154}$$

$$\frac{\partial hRP}{\partial t} = -\frac{a^2}{r^2}\left(2W + h \frac{\partial U}{\partial x} \right) \tag{155}$$

Adding the assumption of a weak nonlinearity, i.e. the water elevation is very small compared to the still water depth, which is satisfied for a tsunami in deep waters (but not in shallow waters), h can be treated as a constant with respect to t thanks to (152) as well as with respect to x (on a constant bottom) and the acoustic subsystem can be written

$$\frac{\partial \overline{\mathbf{V}}}{\partial t} + \overline{\overline{\mathbf{A}}}_{\mathbf{A}} \frac{\partial \overline{\mathbf{V}}}{\partial x} = \overline{\mathbf{S}} \tag{156}$$

where

$$\overline{\overline{\mathbf{A}}}_{\mathbf{A}} = \begin{bmatrix} 0 & 0 & 0 & 0 \\ 0 & 0 & 0 & 1/R \\ 0 & 0 & 0 & 0 \\ 0 & a^2/(r^2 R) & 0 & 0 \end{bmatrix}. \tag{157}$$

The eigenvalues are $\lambda_{1,2} = 0$ and $\lambda_{3,4} = \pm a/(rR) = \pm a_{\text{eff}}$. There is four linearly independent eigenvectors and the system is also hyperbolic. The non-zero characteristics of the system are the effective sound velocity in both directions, hence the name "acoustic" of this subsystem.

With the weak nonlinearity assumption, deriving (155) with respect to t and (153) with respect to x and using (154) leads to an equation for the average non-hydrostatic pressure alone

$$\frac{\partial^2 P}{\partial t^2} - a_{\text{eff}}^2 \frac{\partial^2 P}{\partial x^2} + 3\frac{a_{\text{eff}}^2}{h^2} P = 0. \tag{158}$$

This equation is the Klein-Gordon equation which is the classic example of a hyperbolic-dispersive equation (Whitham 1974). The celerity of the propagation of the acoustic waves is the effective sound velocity and the dispersion relation can be written

$$k^2 = \frac{\omega^2 - \omega_c^2}{a_{\text{eff}}^2} \tag{159}$$

where ω_c is the cutoff angular frequency

$$\omega_c = \frac{a\sqrt{3}}{rhR} \tag{160}$$

which coincides with the cutoff frequency of the acoustic branch (119). If the frequency is smaller than the cutoff frequency, the acoustic wave is evanescent. The cutoff frequency decreases if the depth increases. An acoustic wave can propagate in an ocean if the depth is large enough but can be reflected if the depth decreases. This means that an acoustic mode can be excited in the complete system if the initial conditions include sufficiently high frequencies in an area where the depth is large.

The expression of the phase velocity is

$$v_\varphi = \frac{a_{\text{eff}}}{\sqrt{1 - \omega_c^2/\omega^2}}, \tag{161}$$

which implies that the phase velocity of the acoustic waves is larger than the effective sound velocity (with $v_\varphi \to \infty$ if $\omega \to \omega_c$). Since the classical relation $v_\varphi v_g = a_{\text{eff}}^2$ is satisfied, the group velocity of the acoustic waves is smaller than the effective sound velocity. This is of course the same behaviour as the acoustic branch (see §2.5 and Figure 2).

3 Soliton

The system (90)–(93) admits soliton solutions. A soliton propagates at a constant velocity c and is thus a stationary solution in a reference frame in translation at this velocity with respect

to the reference frame of the bottom. We are looking for a function of the variable $\xi = x - ct$ satisfying $h \to h_\infty$, $U \to 0$, $W \to 0$, $P \to 0$ and $R \to R_\infty$ if $\xi \to \pm\infty$ where U is the average horizontal velocity in the reference frame of the bottom and R_∞ is the value of R for $h = h_\infty$.

Given that $\partial/\partial t = -c\mathrm{d}/\mathrm{d}\xi$ and $\partial/\partial x = \mathrm{d}/\mathrm{d}\xi$, the mass conservation equation (90) implies that the relative discharge

$$\overline{m} = hR\,(U - c) \tag{162}$$

is a constant. The momentum balance equation in the horizontal direction (91) yields another constant B defined by

$$B = \frac{\overline{m}^2}{hR} + Q_1 \frac{gh^2}{2} + hP. \tag{163}$$

The energy equation (77) gives a third constant $\overline{H}$, which writes

$$\overline{H} = \frac{\overline{m}^2}{2h^2R^2} + \frac{2}{3}W^2 + gh + r^2\frac{P^2}{2a^2} + \frac{P}{R}. \tag{164}$$

The expression of the non-hydrostatic pressure can be found from (163):

$$P = \frac{B}{h} - \frac{\overline{m}^2}{h^2R} - Q_1\frac{gh}{2}. \tag{165}$$

The non-hydrostatic pressure equation (92) and the expression of P above gives an expression for the average vertical velocity

$$W = \overline{m}\left(\frac{Q_4}{2h} + \frac{r^2B}{2a^2h^2} - Q_5\frac{r^2\overline{m}^2}{a^2h^3} + Q_1\frac{r^2g}{4a^2}\right)\frac{\mathrm{d}h}{\mathrm{d}\xi} \tag{166}$$

where

$$Q_4 = \frac{M^4}{4\sinh^2(M^2/2)} = 1 + O(M^4) \tag{167}$$

and

$$Q_5 = \frac{M^2}{2}\frac{\left(1+M^2\right)\mathrm{e}^{M^2} - 1}{\left(\mathrm{e}^{M^2} - 1\right)^2} = 1 - \frac{M^2}{4} + O(M^4). \tag{168}$$

The equations are put into dimensionless form by defining $\hat{h} = h/h_\infty$, $\hat{\xi} = \xi/h_\infty$, $\hat{P} = P/gh_\infty$ and two dimensionless numbers, the Mach number $M_\infty = \sqrt{gh_\infty}/a$ and the relative Froude number $\overline{F}_\infty = -\overline{m}/\sqrt{gh_\infty^3}$. The constants B and $\overline{H}$ can be evaluated for $\xi \to \pm\infty$. This gives

$$B = gh_\infty^2\left(\frac{\overline{F}_\infty^2}{R_\infty} + \frac{Q_{1\infty}}{2}\right), \quad \overline{H} = gh_\infty\left(\frac{\overline{F}_\infty^2}{2R_\infty^2} + 1\right), \tag{169}$$

where $Q_{1\infty}$ is the value of Q_1 for $h = h_\infty$. These expressions, used with the energy conservation (164) and the expressions (165) and (166) of P and W, lead to the equation

$$f_1^2(\hat{h})\left(\frac{\mathrm{d}\hat{h}}{\mathrm{d}\hat{\xi}}\right)^2 - f_2(\hat{h}) = 0 \tag{170}$$

where

$$f_1(\hat{h}) = \frac{\overline{F}_\infty}{\sqrt{3}}\left[Q_4 + r^2\frac{M_\infty^2}{\hat{h}}\left(\frac{\overline{F}_\infty^2}{R_\infty} + \frac{Q_{1\infty}}{2}\right) - 2r^2\frac{M_\infty^2}{\hat{h}^2}Q_5\overline{F}_\infty^2 + r^2Q_1\frac{M_\infty^2}{2}\hat{h}\right] \tag{171}$$

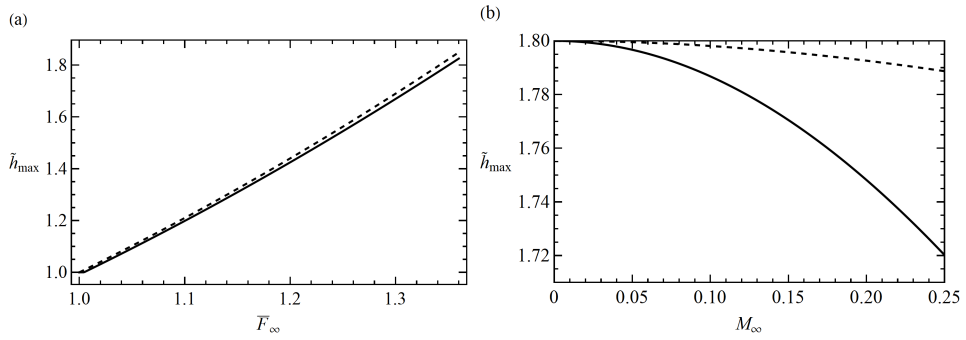

Figure 5: Dimensionless maximum depth of the soliton (a) as a function of $\overline{F}_\infty$ for $M_\infty = 0.13$ (solid curve) and (b) as a function of M_∞ for $\overline{F}_\infty^2 = 1.8$ (solid curve). The dashed curve is in (a) the maximum depth of the soliton of the Serre-Green-Naghdi equations and in (b) the maximum depth in the quasi-incompressible case.

and

$$f_2(\hat{h}) = \frac{\overline{F}_\infty^2}{R^2} - \frac{Q_2}{R}\hat{h}^3 - \left(2\frac{\overline{F}_\infty^2}{R_\infty} + Q_{1\infty}\right)\frac{\hat{h}}{R} + \left(\frac{\overline{F}_\infty^2}{R_\infty^2} + 2\right)\hat{h}^2 - r^2 M_\infty^2 \left(\frac{\overline{F}_\infty^2}{R_\infty} + \frac{Q_{1\infty}}{2} - \frac{\overline{F}_\infty^2}{\hat{h}R} - Q_1\frac{\hat{h}^2}{2}\right)^2. \quad (172)$$

For the maximum depth $h_{\max}$ of the solitary wave, $f_2(\hat{h}) = 0$. Apart from the root $\hat{h} = 1$, the positive root of this equation gives the maximum depth of the soliton. The dimensionless amplitude of the soliton is $h_{\max} - 1$. If $M_\infty = 0$, the maximum depth of the soliton of the Serre-Green-Naghdi equations is recovered. If M_∞ increases, the amplitude of the soliton decreases. This implies that the soliton of the compressible model is slightly smaller than the soliton of the incompressible model (see Figure 5(a) for a comparison between the incompressible and compressible cases for $M_\infty = 0.13$). The soliton of the incompressible equations exists if $\overline{F}_\infty > 1$. There is also a minimum value of the Froude number for the existence of the soliton of the compressible equations and this value is slightly greater than 1 (about $\overline{F}_\infty > 1.004$ if $M_\infty = 0.13$). The maximum depth of the soliton as a function of the Mach number M_∞ is presented in Figure 5(b) for a Froude number $\overline{F}_\infty \simeq 1.342$ ($\overline{F}_\infty^2 = 1.8$). The dashed curve is the quasi-incompressible case. As the quasi-incompressible case is a hyperbolic approximation of the incompressible Serre-Green-Naghdi equations, the value of the sound velocity should be chosen large enough to give approximately the same amplitude as the incompressible model (i.e. M_∞ should be small enough). Note that in the quasi-incompressible case, M_∞ appears only because of the presence of the sound velocity in the relaxation term in (93). The problem is completely different for the compressible equations (90)–(93), which are not an approximation of the incompressible equations, and where the slight decrease of the soliton amplitude is due to the inclusion of compressibility in the model.

Taking the derivative of the equation (170) leads to the equation

$$\frac{\mathrm{d}^2\hat{h}}{\mathrm{d}\hat{\xi}^2} + \frac{1}{f_1(\hat{h})}\frac{\mathrm{d}f_1}{\mathrm{d}\hat{h}}\left(\frac{\mathrm{d}\hat{h}}{\mathrm{d}\hat{\xi}}\right)^2 - \frac{1}{2f_1^2(\hat{h})}\frac{\mathrm{d}f_2}{\mathrm{d}\hat{h}} = 0 \quad (173)$$

which is more suitable for a numerical integration. The depth profile of a very steep soliton with $\overline{F}_\infty^2 = 1.8$ and $M_\infty = 0.13$ is presented in Figure 6(a) (solid curve). This profile is very similar to the profile of the Serre-Green-Naghdi soliton (dashed curve) for the same Froude number.

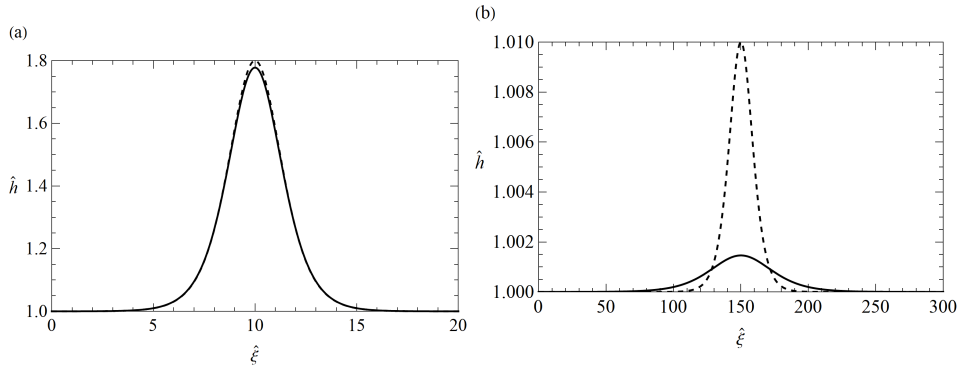

Figure 6: Profile of a soliton for the compressible equations with $M_\infty = 0.13$ (solid curve) and for the Serre-Green-Naghdi equations (dashed curve). (a) $\overline{F}^2_\infty = 1.8$. (b) $\overline{F}^2_\infty = 1.01$.

This soliton has a very large amplitude for an important Mach number, and thus a large still water depth, which is not realistic. A more realistic soliton in a large depth, with $\overline{F}^2_\infty = 1.01$ and $M_\infty = 0.13$, is presented in Figure 6 (b) (solid curve) with a comparison to the Serre-Green-Naghdi soliton at the same Froude number (dashed curve). The decrease in amplitude due to compressibility is notable.

4 Numerical scheme

The terms of the equations (90)–(93) can be gathered into slow terms pertaining to usual shallow water surface waves propagation and into fast terms related to non-hydrostatic ("acoustic") wave propagation:

$$\frac{\partial h}{\partial t} + \underbrace{\frac{\partial hU}{\partial x}}_{\text{slow}} = \underbrace{\frac{M^2}{2} Q_0 h \frac{\partial U}{\partial x}}_{\text{slow / source term}} , \tag{174}$$

$$\frac{\partial hRU}{\partial t} + \underbrace{\frac{\partial}{\partial x}\left(hRU^2 + Q_1 \frac{gh^2}{2}\right)}_{\text{slow}} = - \underbrace{\frac{\partial hP}{\partial x}}_{\text{fast/slow}} , \tag{175}$$

$$\frac{\partial hRW}{\partial t} + \underbrace{\frac{\partial hRUW}{\partial x}}_{\text{slow}} = \underbrace{\frac{3}{2} P}_{\text{fast}}, \tag{176}$$

$$\frac{\partial hRP}{\partial t} + \underbrace{\frac{\partial hRUP}{\partial x}}_{\text{slow}} = \underbrace{-\frac{a_0^2}{r^2}\left(2W + h\frac{\partial U}{\partial x}\right)}_{\text{fast}} . \tag{177}$$

This partitioning is similar to the treatment of the compressible Boussinesq equations by Weller *et al.* (2013) for weather forecasting applications. The numerical motivation of this partitioning is to treat the slow terms explicitly and the fast terms implicitly. The term marked as fast/slow is normally included into the fast acoustic part. This leads to a semi-implicit scheme where the implicit step necessitates to solve a global linear system. This is not ideal given that one of the motivations of this work is to remove the resolution of a global system implied by the elliptic step of the incompressible models. Another possibility is to treat the fast/slow term as a slow term and thus to include it in the explicit part of the scheme. This is analogous to the Horizontally Explicit Vertically Implicit (HEVI) UfPreb (U forward, Pressure backward) splitting of Weller *et al.* (2013). This forward-backward approach is based on Mesinger (1977)

and is a long-established practice for atmospheric models. In our case, the huge advantage of this approach is that no resolution of a global system is needed in the implicit step, which becomes computationally very cheap. In fact, with this splitting, the implicit step is cheaper than the explicit step in computational time.

A numerical scheme of first order being too diffusive, a second-order scheme has to be implemented. The second order in space was obtained with a monotone upstream-centred scheme for conservation laws (MUSCL). Following Tkachenko (2020) on a similar system, the second order in time was achieved with the diagonally-implicit Runge-Kutta (DIRK) Implicit-Explicit (IMEX) ARS2(2,2,2) scheme of Ascher *et al.* (1997) (using the notation of Pareschi & Russo 2005). The additive Runge-Kutta (ARK) IMEX scheme ARK2(2,3,2) of Giraldo *et al.* (2013) was also tested with identical results. The ARS2(2,2,2) has two explicit stages and two implicit stages. The system is written

$$\frac{\partial \overline{\mathbf{U}}}{\partial t} = \mathbf{s}(\overline{\mathbf{U}}) + \mathbf{f}(\overline{\mathbf{U}}), \tag{178}$$

where $\overline{\mathbf{U}} = (h, hRU, hRW, hRP)^{\mathrm{T}}$ and where $\mathbf{s}$ corresponds to the slow terms and $\mathbf{f}$ to the fast terms. The first explicit stage of the IMEX scheme ARS2(2,2,2) can be written

$$\overline{\mathbf{U}}_{\mathbf{1}}^{\dagger} = \overline{\mathbf{U}}^{\mathbf{n}} + \gamma \Delta t\, \mathbf{s}\left(\overline{\mathbf{U}}^{\mathbf{n}}\right) \tag{179}$$

where $\overline{\mathbf{U}}^{\mathbf{n}}$ is $\overline{\mathbf{U}}$ at iteration n and time t_n, Δt is the time step and $\gamma = 1 - \sqrt{2}/2$. The first implicit stage follows with $\overline{\mathbf{U}}_{\mathbf{1}}$ being computed from $\overline{\mathbf{U}}_{\mathbf{1}}^{\dagger}$ by the implicit procedure and a time step $\gamma \Delta t$. The second explicit stage is then

$$\overline{\mathbf{U}}_{\mathbf{2}}^{\dagger} = \overline{\mathbf{U}}^{\mathbf{n}} + \delta \Delta t\, \mathbf{s}\left(\overline{\mathbf{U}}^{\mathbf{n}}\right) + (1-\delta)\, \Delta t\, \mathbf{s}\left(\overline{\mathbf{U}}_{\mathbf{1}}\right) + (1-\gamma)\, \Delta t\, \mathbf{f}\left(\overline{\mathbf{U}}_{\mathbf{1}}\right) \tag{180}$$

with $\delta = -\sqrt{2}/2$. The second implicit stage is the final stage and calculates, at iteration $n+1$ and time $t_{n+1} = t_n + \Delta t$, $\overline{\mathbf{U}}^{\mathbf{n+1}}$ from $\overline{\mathbf{U}}_{\mathbf{2}}^{\dagger}$ by the implicit procedure and a time step $\gamma \Delta t$.

The implicit procedure is a backward Euler method. For a time step $\gamma \Delta t$, the state $\overline{\mathbf{U}} = (h, hRU, hRW, hRP)^{\mathrm{T}}$ ($\overline{\mathbf{U}}_{\mathbf{1}}$ in the first implicit stage and $\overline{\mathbf{U}}^{\mathbf{n+1}}$ in the second implicit stage) is obtained from a state $\overline{\mathbf{U}}^{\dagger} = [h^{\dagger}, (hRU)^{\dagger}, (hRW)^{\dagger}, (hRP)^{\dagger}]^{\mathrm{T}}$ ($\overline{\mathbf{U}}_{\mathbf{1}}^{\dagger}$ or $\overline{\mathbf{U}}_{\mathbf{2}}^{\dagger}$ respectively) by the relations (Δx being the mesh size)

$$h_i = h_i^{\dagger}, \tag{181}$$

$$(hRU)_i = (hRU)_i^{\dagger}, \tag{182}$$

$$(hRW)_i = \frac{1}{1 + \dfrac{3a^2}{r^2 h_i^{\dagger 2} R_i^{\dagger 2}} (\gamma \Delta t)^2} \left[(hRW)_i^{\dagger} + \frac{3}{2} P_i^{\dagger} \gamma \Delta t - \frac{3}{4} \frac{a^2}{r^2 R_i^{\dagger}} \frac{(\gamma \Delta t)^2}{\Delta x} \left(U_{i+1}^{\dagger} - U_{i-1}^{\dagger} \right) \right], \tag{183}$$

$$(hRP)_i = \frac{1}{1 + \dfrac{3a^2}{r^2 h_i^{\dagger 2} R_i^{\dagger 2}} (\gamma \Delta t)^2} \left[(hRP)_i^{\dagger} - 2 \frac{a^2}{r^2} W_i^{\dagger} \gamma \Delta t - \frac{a^2}{2r^2} h_i^{\dagger} \frac{\gamma \Delta t}{\Delta x} \left(U_{i+1}^{\dagger} - U_{i-1}^{\dagger} \right) \right]. \tag{184}$$

The equation (181) implies $R_i = R_i^{\dagger}$ and, together with (182), implies $U_i = U_i^{\dagger}$. The derivative $\partial U / \partial x$ is calculated by a central finite difference method.

In the explicit stages, the slow terms are computed by a finite volume method (Godunov-type) and a Rusanov Riemann solver, except that the term $\partial(hP)/\partial x$ is treated as a source term by a central finite difference. This preserves the classical Saint-Venant (shallow water) structure of equations (with compressible corrections) with the fluxes $\mathbf{F} = (hU, hRU^2 + Q_1 g h^2/2, hRUW, hRUP)^{\mathrm{T}}$. However this term could be also included in the hyperbolic fluxes calculated with the Riemann solver. A Harten-Lax-van Leer (HLL) Riemann solver was also

tested with identical results. The time step is calculated by a standard Courant-Friedrichs-Levy (CFL) condition with the characteristics $U \pm \sqrt{\exp(-M^2)(ghR+P)+a^2/(r^2R^2)}$, which can be practically approximated by $U \pm \sqrt{gh+a^2/r^2}$ for this purpose. A Courant number equal to 0.8 was used in the computations. The Rusanov intercell flux $\mathbf{F}_{i+1/2}$ between a left cell (flux $\mathbf{F}_i$, state $\overline{\mathbf{U}}_i$) and a right cell (flux $\mathbf{F}_{i+1}$, state $\overline{\mathbf{U}}_{i+1}$) is calculated by

$$\mathbf{F}_{i+1/2} = \frac{1}{2}\left(\mathbf{F}_i + \mathbf{F}_{i+1}\right) - \frac{1}{2}S_+\left(\overline{\mathbf{U}}_{i+1} - \overline{\mathbf{U}}_i\right) \tag{185}$$

where the structure of the fluxes enables to calculate S_+ with the classical incompressible shallow water characteristics, as $\max(|U_{i+1}+\sqrt{gh_{i+1}}|, |U_i+\sqrt{gh_i}|, |U_{i+1}-\sqrt{gh_{i+1}}|, |U_i-\sqrt{gh_i}|)$. In fact, due to the compressible corrections, S_+ is slightly overestimated. The calculation of the slow terms can be written for the cell i

$$\mathbf{s}(\overline{\mathbf{U}})_i = \frac{\mathbf{F}_{i-1/2} - \mathbf{F}_{i+1/2}}{\Delta x} + \begin{pmatrix} M_i^2 Q_{0i} h_i \left(U_{i+1} - U_{i-1}\right)/(4\Delta x) \\ -\left[(hP)_{i+1} - (hP)_{i-1}\right]/(2\Delta x) \\ 0 \\ 0 \end{pmatrix} \tag{186}$$

The fast terms in the second explicit stage (180) are calculated by a forward Euler method, which gives for the cell i

$$\mathbf{f}\left(\overline{\mathbf{U}}\right)_i = \begin{pmatrix} 0 \\ 0 \\ \frac{3}{2}P_i \\ -2\frac{a^2}{r^2}W_i - \frac{a^2 h_i}{2r^2\Delta x}\left(U_{i+1} - U_{i-1}\right) \end{pmatrix} \tag{187}$$

4.1 Numerical simulations

This numerical scheme is used to simulate the propagation of a soliton. First, $h_{\max}$ and h_∞ are chosen. This gives the value of M_∞, R_∞ and $Q_{1\infty}$. The value of the Froude number $\overline{F}_\infty$ is found by solving the equation $f_2(\hat{h}) = 0$ (see (172)). The initial condition is the soliton solution obtained by the numerical resolution of the ordinary differential equation (173). This gives the initial depth profile $h(x, t=0)$ of the wave as well as the initial derivative $\partial h/\partial x$. The initial conditions on the other variables are then calculated by

$$U = \overline{F}_\infty \frac{\sqrt{gh_\infty}}{R_\infty}\left(1 - \frac{h_\infty R_\infty}{hR}\right), \tag{188}$$

$$P = \left(\frac{\overline{F}_\infty^2}{R_\infty} + \frac{Q_{1\infty}}{2}\right)\frac{gh_\infty^2}{h} - \overline{F}_\infty^2 \frac{gh_\infty^3}{h^2 R} - Q_1 \frac{gh}{2}, \tag{189}$$

and

$$W = \frac{\overline{F}_\infty \sqrt{gh_\infty^3}}{2}\left[2r^2 Q_5 \frac{\overline{F}_\infty^2}{a^2}\frac{gh_\infty^3}{h^3} - \left(\frac{\overline{F}_\infty^2}{R_\infty} + \frac{Q_{1\infty}}{2}\right)\frac{r^2 gh_\infty^2}{a^2 h^2} - Q_1 \frac{gr^2}{2a^2} - \frac{Q_4}{h}\right]\frac{\partial h}{\partial x}. \tag{190}$$

To study the propagation of the solitary wave in its own reference frame, the initial horizontal velocity is

$$U = -\overline{F}_\infty \frac{h_\infty \sqrt{gh_\infty}}{hR}. \tag{191}$$

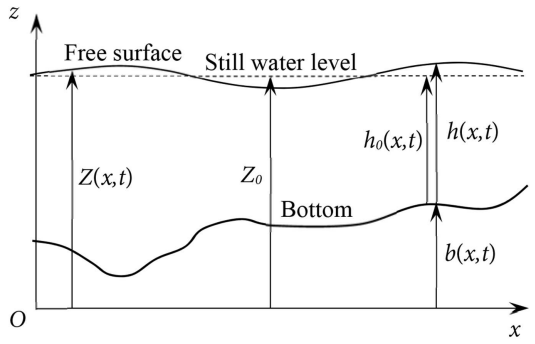

Figure 7: Notations used in the text.

The attenuation of a solitary wave with an initial amplitude of 4.79 m propagating in a large depth of $h_\infty = 4000\,\mathrm{m}$ is studied with $\overline{F}_\infty \simeq 1.005$ and $M_\infty \simeq 0.132$. The simulation time is 2 h 36 min in a periodic box of length 1600 km. The diminution of the soliton's amplitude is of 1.04 % for a cell size $\Delta x = 8\,\mathrm{km}$ and decreases to 0.02 % for $\Delta x = 2\,\mathrm{km}$ and to 0.006 % for $\Delta x = 1\,\mathrm{km}$. With the same initial amplitude, depth, Froude and Mach numbers, in a non-periodic domain of 2400 km with two sponge layers on each side, after a simulation time of 5 h 12 min in the reference frame of the soliton and $\Delta x = 1\,\mathrm{km}$, the amplitude of the soliton has decreased of only 0.009 %. A cell size of 1 km is thus likely to be appropriate for the simulation of a tsunami in a deep ocean of approximately constant depth.

5 Equations with an arbitrary bathymetry

The case of a variable and mobile bottom is treated with a similar method. Some details of the derivation are presented in Appendix A. Only the main results are given in this section.

The bathymetry is measured by the elevation $b(x,t)$ of the bottom over a constant horizontal datum. Since the seabed can be displaced due to seismic effects, the bottom can be mobile and b depends on t. The still water depth above the bottom is denoted by $h_0(x,t)$ and the total water depth by $h(x,t)$. The elevation of the free surface over the horizontal datum is $Z(x,t) = h(x,t) + b(x,t)$. The elevation of the free surface at rest over the horizontal datum is a constant Z_0 which can be chosen equal to zero (the horizontal datum is the still water level). In this case, $b = -h_0$ and Z is equal to the wave elevation $\eta = h - h_0$. The notations are presented in Figure 7. There is no particular smallness assumption on b nor on its derivatives. In particular, the characteristic variation length of b in the Ox-direction is L (see §2.2).

5.1 Mass and momentum balance equations

The expression of the average density R is unchanged and given by (49). The depth-averaged mass conservation equation is also not modified and can be written in the equivalent forms (94) or (90). The depth-averaged momentum balance equation in the Ox-direction can be written

$$\frac{\partial hR\mathcal{U}}{\partial t} + \frac{\partial}{\partial x}\left(hRU\mathcal{U} + Q_1\frac{gh^2}{2} + hP\right) = -\left(ghR + 2P\right)\frac{\partial b}{\partial x} + hR\frac{\dot{b} - W}{3}\frac{\mathrm{D}}{\mathrm{D}t}\left(\frac{\partial b}{\partial x}\right) \tag{192}$$

where $\mathcal{U}$ is a modified average horizontal velocity defined by

$$\mathcal{U} = U + \frac{\dot{b} - W}{3}\frac{\partial b}{\partial x} \tag{193}$$

and where the material derivative is defined as

$$\dot{b} = \frac{\mathrm{D}b}{\mathrm{D}t} = \frac{\partial b}{\partial t} + U\frac{\partial b}{\partial x}. \tag{194}$$

In the same way, the depth-averaged momentum balance equation in the Oz-direction is written

$$\frac{\partial hR\mathcal{W}}{\partial t} + \frac{\partial hRU\mathcal{W}}{\partial x} = \frac{3}{2}P \tag{195}$$

where the modified average vertical velocity is

$$\mathcal{W} = W - \frac{\dot{b}}{4}. \tag{196}$$

5.2 Energy conservation

Due to the mobile bottom, the total energy of the system is not conserved because the external forces do work. The expression of the power of the external forces is

$$\mathcal{P}_{\text{ext}} = ghR\frac{\partial b}{\partial t} + \left[2P + \frac{hR}{3}\frac{\mathrm{D}}{\mathrm{D}t}\left(\dot{b} - W\right)\right]\frac{\partial b}{\partial t}. \tag{197}$$

Of course, this power is equal to zero if the bottom is not mobile i.e. if $\partial b/\partial t = 0$. In this expression, the first term is due to the hydrostatic pressure and the second term is due to the non-hydrostatic pressure, in both cases evaluated at the bottom ($z = b$). The power of the internal forces can be written

$$\mathcal{P}_{\text{int}} = P\left(2W + h\frac{\partial U}{\partial x} - 2\dot{b}\right). \tag{198}$$

It can be noted that the term $2P\partial b/\partial t$ in $\mathcal{P}_{\text{ext}}$ is exactly compensated by a term $-2P\partial b/\partial t$ in $\mathcal{P}_{\text{int}}$. This means that this part of the power of the external forces is immediately transferred to the internal energy through the power of the internal forces. The other terms of $\mathcal{P}_{\text{ext}}$ appear in the mechanical energy balance equation which writes

$$\frac{\partial hRe_M}{\partial t} + \frac{\partial}{\partial x}\left(hRUe_M + \Pi U\right) = \mathcal{P}_{\text{int}} + \mathcal{P}_{\text{ext}} \tag{199}$$

where Π is given by (76) and where the expression of the mechanical energy is

$$e_M = \frac{U^2}{2} + \frac{W^2}{2} + \frac{\left(W - \dot{b}\right)^2}{6} + \frac{Q_2}{R}\frac{gh}{2} + gb. \tag{200}$$

The term gb is included in the potential energy since the average elevation of the flow over the horizontal datum is $b + h/2$. However the non-uniformity of the density due to compressibility is responsible for the factor Q_2/R. The average kinetic energy includes a term $\langle w^2/2\rangle$. Decomposing the vertical velocity as $w = W + w'$ leads to $\langle w^2\rangle = W^2 + \langle w'^2\rangle$. The last term can be written to within negligible terms

$$\langle w'^2\rangle = \frac{\left(W - \dot{b}\right)^2}{3}. \tag{201}$$

The third term in the right-hand side of (200) is thus $\langle w'^2\rangle/2$, and, together with the second term, represents $\langle w^2/2\rangle$.

Averaging over the depth the first law of thermodynamics (9) leads to the average total energy balance equation

$$\frac{\partial hRe}{\partial t} + \frac{\partial}{\partial x}\left(hRUe + \Pi U\right) = \mathcal{P}_{\text{ext}} \tag{202}$$

where the total energy is the sum of the mechanical energy and the internal energy

$$e = e_M + e_i, \tag{203}$$

the expression of the internal energy being

$$e_i = \frac{r^2 P^2}{2a^2} \tag{204}$$

with $r = \sqrt{6/5}$ (but this value can be artificially increased in some cases to decrease the computational time). The system satisfies an exact energy balance equation, even on an arbitrary topography.

The equation for the average non-hydrostatic pressure can be deduced from the energy equation. It writes

$$\frac{\partial hRP}{\partial t} + \frac{\partial hRUP}{\partial x} = -\frac{a^2}{r^2}\left(2W + h\frac{\partial U}{\partial x} - 2\dot{b}\right). \tag{205}$$

In the particular case of a mild slope, the characteristic variation length of b in the Ox-direction is supposed to be very large and of $O(L/\varepsilon)$. The mass equation (90) is unchanged. The average momentum balance equation in the Oz-direction and the equation for the average non-hydrostatic pressure are the same as for a constant bottom, (92) and (93) respectively, and the average momentum balance equation in the Ox-direction writes

$$\frac{\partial hRU}{\partial t} + \frac{\partial}{\partial x}\left(hRU^2 + Q_1\frac{gh^2}{2} + hP\right) = -ghR\frac{\partial b}{\partial x}. \tag{206}$$

All other terms due to the variable bottom become of $O(\varepsilon^3)$ or smaller in this scaling. This system admits an exact energy conservation equation with the energy

$$e = \frac{U^2}{2} + \frac{2W^2}{3} + \frac{Q_2}{R}\frac{gh}{2} + gb. \tag{207}$$

Note that, in the quasi-incompressible case or, equivalently, in the hyperbolic counterpart of the Serre-Green-Naghdi equations, the conservation of energy is also satisfied exactly both in the case of an arbitrary bathymetry and in the case of a mild bottom.

5.3 Hyperbolicity

The system can be written

$$\frac{\partial \overline{\mathbf{V}}_\mathbf{B}}{\partial t} + \overline{\overline{\mathbf{A}}}_\mathbf{B}\,\frac{\partial \overline{\mathbf{V}}_\mathbf{B}}{\partial x} = \overline{\mathbf{S}}_\mathbf{B} \tag{208}$$

where $\overline{\mathbf{V}}_\mathbf{B} = (h, \mathcal{U}, \mathcal{W}, P)^{\mathrm{T}}$, $\overline{\mathbf{S}}_\mathbf{B}$ is a source term depending on b and its derivatives, and on h, $\mathcal{U}$, $\mathcal{W}$, P but not on their derivatives, and where

$$\overline{\overline{\mathbf{A}}}_\mathbf{B} = \begin{bmatrix} U & \mathrm{e}^{-M^2}hRK_b & \mathrm{e}^{-M^2}hRK_b(\partial b/\partial x)/3 & 0 \\ g + P/(hR) & U & 0 & 1/R \\ 0 & 0 & U & 0 \\ 0 & K_b a^2/(r^2 R) & K_b a^2(\partial b/\partial x)/(3r^2 R) & U \end{bmatrix}. \tag{209}$$

with

$$K_b = \frac{1}{1 + \frac{1}{4}\left(\frac{\partial b}{\partial x}\right)^2}. \tag{210}$$

The eigenvalues of $\overline{\overline{\mathbf{A_B}}}$ are

$$\lambda_{1,2} = U \; ; \quad \lambda_{3,4} = U \pm \sqrt{K_b}\sqrt{\mathrm{e}^{-M^2}\left(ghR + P\right) + \frac{a^2}{r^2R^2}}. \tag{211}$$

It is possible to find four linearly independent eigenvectors. The eigenvalues are real (since P is always very small and a very large). The system is thus hyperbolic. The free surface waves velocity is smaller with a variable bottom than with a constant bottom since it is multiplied by $\sqrt{K_b}$ and $K_b \leqslant 1$. In practice however, $(\partial b/\partial x)^2$ is often small and the surface wave velocity is only slightly decreased except for very steep bottom slopes. For example, if the bottom slope is 1/10, 1/5 and 1, $\sqrt{K_b}$ is equal to 0.999, 0.995 and 0.894 respectively.

5.4 Well-balanced form of the equations

For the numerical resolution on an arbitrary bathymetry, the system must be well-balanced. The pre-balanced formulation of Liang & Marche (2009) and Duran & Marche (2017) is adapted to the present system of equations. Using the wave elevation $\eta = h - h_0$, the pre-balanced formulation of the full system of equations writes

$$\frac{\partial \eta}{\partial t} + \frac{\partial hU}{\partial x} = \frac{M^2}{2} Q_0 h \frac{\partial U}{\partial x} - \frac{\partial h_0}{\partial t}, \tag{212}$$

$$\begin{aligned} \frac{\partial hR\mathcal{U}}{\partial t} + \frac{\partial}{\partial x}\left[hRU\mathcal{U} + Q_1 g\left(\frac{\eta^2}{2} + h_0\eta\right) + Q_1'\frac{gh_0^2}{2} + hP\right] \\ = \left[g\left(h_0R' + \eta R\right) + 2P\right]\frac{\partial h_0}{\partial x} + \frac{hR}{3}\left(\dot{h}_0 + W\right)\frac{\mathrm{D}}{\mathrm{D}t}\left(\frac{\partial h_0}{\partial x}\right), \end{aligned} \tag{213}$$

$$\frac{\partial hR\mathcal{W}}{\partial t} + \frac{\partial hRU\mathcal{W}}{\partial x} = \frac{3}{2}P, \tag{214}$$

$$\frac{\partial hRP}{\partial t} + \frac{\partial hRUP}{\partial x} = -\frac{a^2}{r^2}\left(2W + h\frac{\partial U}{\partial x} + 2\dot{h}_0\right). \tag{215}$$

In this system, the following quantities are defined:

$$M_0^2 = \frac{gh_0}{a^2} \; ; \quad R_0 = \frac{\mathrm{e}^{M_0^2} - 1}{M_0^2} \; ; \quad Q_{10} = \frac{2}{M_0^4}\left(\mathrm{e}^{M_0^2} - M_0^2 - 1\right) \; ; \tag{216}$$

$$Q_1' = Q_1 - Q_{10} \; ; \quad R' = R - R_0. \tag{217}$$

Once the modified velocities $\mathcal{U}$ and $\mathcal{W}$ have been calculated, it is possible to revert to the average velocities U and W by inverting the relations (193) and (196), which gives

$$U = K_b\left[\mathcal{U} - \left(\frac{\mathcal{W}}{3} + \frac{1}{4}\frac{\partial h_0}{\partial t}\right)\frac{\partial h_0}{\partial x}\right] \tag{218}$$

and

$$W = K_b\left[\mathcal{W} - \frac{\mathcal{U}}{4}\frac{\partial h_0}{\partial x} + \frac{\mathcal{W}}{3}\left(\frac{\partial h_0}{\partial x}\right)^2 - \frac{1}{4}\frac{\partial h_0}{\partial t}\right]. \tag{219}$$

The final system of equations on an arbitrary bathymetry is thus a well-balanced hyperbolic set of only four equations satisfying the exact mass conservation equation (94) and the exact energy balance equation (202) (the total energy is conserved if the bottom is not mobile).

The hyperbolic approximation of the Serre-Green-Naghdi equations of Escalante & Morales de Luna (2020) is a six-equation model (with $B = 0$, $\beta = 1/12$ and $\zeta = 0$ in their notations) which is, according to our terminology, a quasi-incompressible model. This model does not satisfy exactly, but only asymptotically, the conservation of energy, including on a constant bottom.

5.5 Improved dispersive properties

The same method as in §2.6 is used to derive the equations with improved dispersive properties on an arbitrary bathymetry. The variable W^* has the same meaning as in §2.6: it is the value of w at the relative height $\alpha/2$ over the bottom with respect to the fluid depth. The expression of α is

$$\frac{\alpha}{2} = \frac{z-b}{h}. \tag{220}$$

The following system of equations is the generalisation of (135)–(139) for a variable and mobile bottom, with a pre-balanced formulation:

$$\frac{\partial \eta}{\partial t} + \frac{\partial hU}{\partial x} = \frac{M^2}{2} Q_0 h \frac{\partial U}{\partial x} - \frac{\partial h_0}{\partial t}, \tag{221}$$

$$\begin{aligned}\frac{\partial hR\mathcal{U}^*}{\partial t} + \frac{\partial}{\partial x}\left[hRU\mathcal{U}^* + Q_1 g\left(\frac{\eta^2}{2} + h_0\eta\right) + Q_1'\frac{gh_0^2}{2} + hP\right] \\ = \left[g\left(h_0 R' + \eta R\right) + 2P\right]\frac{\partial h_0}{\partial x} + \frac{hR}{3}\left(\dot{h}_0 + W^*\right)\frac{\mathrm{D}}{\mathrm{D}t}\left(\frac{\partial h_0}{\partial x}\right) \\ + \frac{4}{3}\frac{\alpha-1}{\alpha^2}\frac{\partial h_0}{\partial x}\left(W^* + \dot{h}_0\right)^2 + \frac{\alpha-1}{6\alpha} g h^2 R \frac{\partial h_0}{\partial x}\frac{\partial S^*}{\partial x},\end{aligned} \tag{222}$$

$$\frac{\partial hR\mathcal{W}^*}{\partial t} + \frac{\partial hRU\mathcal{W}^*}{\partial x} = \frac{3}{2}R^2 P + \frac{\alpha-1}{2\alpha} g h^2 R \frac{\partial S^*}{\partial x} + 4\frac{\alpha-1}{\alpha^2}\left(W^* + \dot{h}_0\right)^2, \tag{223}$$

$$\frac{\partial hRP}{\partial t} + \frac{\partial hRUP}{\partial x} = -\frac{a^2}{r^2}\left(2R^2 W^* + \alpha h \frac{\partial U}{\partial x} + 2\dot{h}_0\right), \tag{224}$$

$$\begin{aligned}\frac{\partial hRS^*}{\partial t} + \frac{\partial hRUS^*}{\partial x} = \frac{2h}{R^3}\frac{\partial W^*}{\partial x} + \frac{2W^*S^*}{\alpha} - \frac{2}{\alpha}(2-\alpha)W^*\frac{\partial h_0}{\partial x} \\ + (2-\alpha)hR\frac{\mathrm{D}}{\mathrm{D}t}\left(\frac{\partial h_0}{\partial x}\right) + \frac{2\dot{h}_0}{\alpha}\left[S^* - (2-\alpha)\frac{\partial h_0}{\partial x}\right],\end{aligned} \tag{225}$$

where the variable S^* is the slope of the free surface multiplied by α and defined as

$$S^* = \alpha \frac{\partial \eta}{\partial x}. \tag{226}$$

The variables $\mathcal{U}^*$ and $\mathcal{W}^*$ are defined by

$$\mathcal{U}^* = U + \frac{\dot{h}_0 + W^*}{3}\frac{\partial h_0}{\partial x}\ ; \quad \mathcal{W}^* = W^* + \frac{\dot{h}_0}{4}. \tag{227}$$

The inversion of these expressions gives U and W^* by

$$U = K_b\left[\mathcal{U}^* - \left(\frac{\mathcal{W}^*}{3} + \frac{1}{4}\frac{\partial h_0}{\partial t}\right)\frac{\partial h_0}{\partial x}\right] \tag{228}$$

and

$$W^* = K_b\left[\mathcal{W}^* - \frac{\mathcal{U}^*}{4}\frac{\partial h_0}{\partial x} + \frac{\mathcal{W}^*}{3}\left(\frac{\partial h_0}{\partial x}\right)^2 - \frac{1}{4}\frac{\partial h_0}{\partial t}\right]. \tag{229}$$

Note that $b + h_0$ is a constant, which implies that $\partial h_0/\partial x = -\partial b/\partial x$ and $\partial h_0/\partial t = -\partial b/\partial t$. The system can be written

$$\frac{\partial \overline{\mathbf{V}}^*_{\mathbf{B}}}{\partial t} + \overline{\overline{\mathbf{A}}}^*_{\mathbf{B}}\frac{\partial \overline{\mathbf{V}}^*_{\mathbf{B}}}{\partial x} = \overline{\mathbf{S}}^*_{\mathbf{B}} \tag{230}$$

where $\overline{\mathbf{V}}^*_{\mathbf{B}} = (h, \mathcal{U}^*, \mathcal{W}^*, P, S^*)^{\mathrm{T}}$, $\overline{\mathbf{S}}^*_{\mathbf{B}}$ contains no derivatives of h, $\mathcal{U}^*$, $\mathcal{W}^*$, P or S^* and where the matrix $\overline{\overline{\mathbf{A}}}^*_{\mathbf{B}}$ is given by (denoting $b_x = \partial b/\partial x$)

$$\begin{bmatrix} U & K_b \mathrm{e}^{-M^2} hR & K_b \mathrm{e}^{-M^2} b_x hR/3 & 0 & 0 \\ g + P/(hR) & U & 0 & 1/R & (\alpha-1)ghb_x/(6\alpha) \\ 0 & 0 & U & 0 & -(\alpha-1)gh/(2\alpha) \\ 0 & K_b \alpha a^2/(r^2 R) & K_b \alpha a^2 b_x/(3r^2 R) & U & 0 \\ 0 & -K_b b_x/(2R^4) & -2K_b(1 + b_x^2/3)/R^4 & 0 & U \end{bmatrix}. \tag{231}$$

The five eigenvalues of this matrix are

$$\lambda_1 = U \; ; \; \lambda_{2,3} = U \pm \frac{\sqrt{gh}}{R^2}\sqrt{\frac{\alpha-1}{\alpha}} \; ; \; \lambda_{4,5} = U \pm \sqrt{K_b}\sqrt{(ghR + P)\,\mathrm{e}^{-M^2} + \frac{\alpha a^2}{r^2 R^2}}. \tag{232}$$

The system is hyperbolic if $\alpha > 1$, which is the case since the value $\alpha = 1.19$ is used.

The equations with improved dispersive properties on an arbitrary bathymetry form a well-balanced hyperbolic system of equations ($\alpha > 1$) which satisfies exactly the mass conservation equation. The total energy balance equation is exactly satisfied if $\alpha = 1$ but, as usual for this method, only asymptotically if $\alpha \neq 1$.

6 Numerical resolution

6.1 Numerical scheme

The numerical scheme in variable bottom is very similar to the case of a constant depth (§4). The fast subsystem is

$$\frac{\partial \eta}{\partial t} = -\frac{\partial h_0}{\partial t}, \tag{233}$$

which implies $\partial h/\partial t = 0$ and $\partial R/\partial t = 0$,

$$\frac{\partial hRU}{\partial t} = 0, \tag{234}$$

$$\frac{\partial hRW^*}{\partial t} = \frac{3}{2}R^2 P, \tag{235}$$

$$\frac{\partial hRP}{\partial t} = -\frac{a^2}{r^2}\left(2R^2 W^* + \alpha h \frac{\partial U}{\partial x} + 2\dot{h}_0\right), \tag{236}$$

and

$$\frac{\partial hRS^*}{\partial t} = 0. \tag{237}$$

All other terms belong to the slow subsystem. Consequently, in the fast subsystem, $\partial U/\partial t = 0$ and $\partial S^*/\partial t = 0$.

The same second order IMEX ARS2(2,2,2) scheme of Ascher *et al.* (1997) is used but $\overline{\mathbf{U}} = (\eta, hR\mathcal{U}, hR\mathcal{W}, hRP)^{\mathrm{T}}$ if $\alpha = 1$ and $\overline{\mathbf{U}} = (\eta, hR\mathcal{U}^*, hR\mathcal{W}^*, hRP, hRS^*)^{\mathrm{T}}$ if $\alpha \neq 1$. In the following, if $\alpha = 1$, the fifth equation (in the variable S^*) is not solved, being useless, $\mathcal{U}^*$ and $\mathcal{W}^*$ are replaced respectively by $\mathcal{U}$ and $\mathcal{W}$ and the fifth component of each matrix is ignored.

The system being splitted in a slow and fast subsystems as in (178), the expression of the slow part $\mathbf{s}$ is now, at cell i,

$$\mathbf{s}(\overline{\mathbf{U}})_i = \frac{\mathbf{F}_{i-1/2} - \mathbf{F}_{i+1/2}}{\Delta x} + \mathbf{T}_i \tag{238}$$

where the flux is

$$\mathbf{F} = \begin{pmatrix} hU \\ hRU\mathcal{U}^* + Q_1 g\left(\dfrac{\eta^2}{2} + h_0\eta\right) + Q_1'\dfrac{gh_0^2}{2} \\ hRU\mathcal{W}^* \\ hRUP \\ hRUS^* \end{pmatrix} \tag{239}$$

and where its interstitial values are calculated by a Rusanov solver and a MUSCL scheme.

In the source terms, the derivatives of the variables are obtained with a finite difference method accurate to the second order for a non-uniform meshing. This derivative for any quantity A is denoted for the cell i by $\mathrm{d}_{xi}(A)$ and its expression is

$$\mathrm{d}_{xi}(A) = -\frac{x_{i+1}-x_i}{(x_i-x_{i-1})(x_{i+1}-x_{i-1})}A_{i-1} + \frac{x_{i+1}-2x_i+x_{i-1}}{(x_i-x_{i-1})(x_{i+1}-x_i)}A_i + \frac{x_i-x_{i-1}}{(x_{i+1}-x_i)(x_{i+1}-x_{i-1})}A_{i+1} \tag{240}$$

where x_{i-1}, x_i and x_{i+1} are the abscissas of the centres of cells $i-1$, i and $i+1$ respectively and A_{i-1}, A_i and A_{i+1} are the values of the quantity A at these abscissas. This expression reduces to the classical expression $(A_{i+1}-A_{i-1})/(2\Delta x)$ in the case of a uniform meshing.

The value of the still water depth h_0 in cell i is denoted by h_{0i}. The derivatives of h_0 in cell i are denoted thereafter by

$$\begin{aligned} h_{xi}^{(0)} &= \left(\frac{\partial h_0}{\partial x}\right)_i ; \quad h_{ti}^{(0)} = \left(\frac{\partial h_0}{\partial t}\right)_i ; \\ h_{xti}^{(0)} &= \left(\frac{\partial^2 h_0}{\partial x \partial t}\right)_i ; \quad h_{xxi}^{(0)} = \left(\frac{\partial^2 h_0}{\partial x^2}\right)_i ; \quad h_{tti}^{(0)} = \left(\frac{\partial^2 h_0}{\partial t^2}\right)_i . \end{aligned} \tag{241}$$

The components of the source term $\mathbf{T} = (T^{(1)}, T^{(2)}, T^{(3)}, T^{(4)}, T^{(5)})^{\mathrm{T}}$ are, at cell i,

$$T_i^{(1)} = \frac{M_i^2}{2} Q_{0i} h_i \mathrm{d}_{xi}(U), \tag{242}$$

$$\begin{aligned} T_i^{(2)} = -\mathrm{d}_{xi}(hP) + [g(h_{0i}R_i' + \eta_i R_i) + 2P_i]h_{xi}^{(0)} \\ + \frac{h_i R_i}{3}(h_{ti}^{(0)} + U_i h_{xi}^{(0)} + W_i^*)(h_{xti}^{(0)} + U_i h_{xxi}^{(0)}) \\ + \frac{4}{3}\frac{\alpha-1}{\alpha^2}h_{xi}^{(0)}\left(W_i^* + h_{ti}^{(0)} + U_i h_{xi}^{(0)}\right)^2 + \frac{\alpha-1}{6\alpha} g h_i^2 R_i h_{xi}^{(0)} \mathrm{d}_{xi}(S^*), \end{aligned} \tag{243}$$

$$T_i^{(3)} = \frac{\alpha-1}{2\alpha} g h_i^2 R_i \mathrm{d}_{xi}(S^*) + 4\frac{\alpha-1}{\alpha^2}\left(W_i^* + h_{ti}^{(0)} + U_i h_{xi}^{(0)}\right)^2, \tag{244}$$

$$T_i^{(4)} = 0, \tag{245}$$

$$\begin{aligned} T_i^{(5)} = \frac{2h_i}{R_i^3}\mathrm{d}_{xi}(W^*) + \frac{2}{\alpha}W_i^* S_i^* - \frac{2}{\alpha}(2-\alpha)W_i^* h_{xi}^{(0)} + (2-\alpha)h_i R_i\left(h_{xti}^{(0)} + U_i h_{xxi}^{(0)}\right) \\ + \frac{2}{\alpha}\left(h_{ti}^{(0)} + U_i h_{xi}^{(0)}\right)\left[S_i^* - (2-\alpha)\, h_{xi}^{(0)}\right]. \end{aligned} \tag{246}$$

In the second explicit step, the fast term, which is calculated by a forward Euler method as in §4, is, at cell i

$$\mathbf{f}\left(\overline{\mathbf{U}}\right)_i = \begin{pmatrix} -h_{ti}^{(0)} \\ \frac{R_i^2}{2} h_{xi}^{(0)} P_i + \frac{h_i R_i}{3}\left[\left(h_{ti}^{(0)} + 2U_i h_{xi}^{(0)} + W_i^*\right) h_{xti}^{(0)} + h_{xi}^{(0)} h_{tti}^{(0)}\right] \\ \frac{3}{2} R_i^2 P_i + \frac{h_i R_i}{4}\left(h_{tti}^{(0)} + U_i h_{xti}^{(0)}\right) \\ -\frac{a^2}{r^2}\left(2R_i^2 W_i^* + \alpha h_i \mathrm{d}_{xi}(U) + 2h_{ti}^{(0)} + 2U_i h_{xi}^{(0)}\right) \\ 0 \end{pmatrix} \tag{247}$$

In the implicit procedure, for a time step $\gamma\Delta t$ and a mesh size Δx, the state $\overline{\mathbf{U}}$ is obtained from a state $\overline{\mathbf{U}}^\dagger = [\eta^\dagger, (hR\mathcal{U}^*)^\dagger, (hR\mathcal{W}^*)^\dagger, (hRP)^\dagger, (hRS^*)^\dagger]^{\mathrm{T}}$ by a backward Euler method, which gives (h, U and S^* being constant in this step)

$$\eta_i = \eta_i^\dagger - h_{ti}^{(0)} \gamma\Delta t, \tag{248}$$

$$(hRW^*)_i = \frac{1}{1 + \dfrac{3a^2 R_i^{\dagger 2}}{r^2 h_i^{\dagger 2}} (\gamma\Delta t)^2} \left[(hRW^*)_i^\dagger + \frac{3}{2} R_i^{\dagger 2} P_i^\dagger \gamma\Delta t \right.$$
$$\left. -\frac{3}{2}\alpha\frac{a^2}{r^2} R_i^\dagger \mathrm{d}_{xi}(U^\dagger) (\gamma\Delta t)^2 - 3\frac{a^2}{r^2}\frac{R_i^\dagger}{h_i^\dagger}\left(h_{ti}^{(0)} + U_i^\dagger h_{xi}^{(0)}\right)(\gamma\Delta t)^2 \right], \tag{249}$$

$$(hRP)_i = \frac{1}{1 + \dfrac{3a^2 R_i^{\dagger 2}}{r^2 h_i^{\dagger 2}} (\gamma\Delta t)^2} \left[(hRP)_i^\dagger - 2\frac{a^2}{r^2} R_i^{\dagger 2} W_i^{*\dagger} \gamma\Delta t \right.$$
$$\left. -\alpha\frac{a^2}{r^2} h_i^\dagger \mathrm{d}_{xi}(U^\dagger)\gamma\Delta t - 2\frac{a^2}{r^2}\left(h_{ti}^{(0)} + U_i^\dagger h_{xi}^{(0)}\right)\gamma\Delta t \right]. \tag{250}$$

The main steps of the numerical resolution are thus

- Calculate $\mathbf{s}(\overline{\mathbf{U}}^{\mathbf{n}})$;
- Compute the first explicit stage as per (179);
- Extract U and W^* from $\mathcal{U}^*$ and $\mathcal{W}^*$ with (228) and (229);
- Compute the first implicit stage with (248), (249) and (250) and extract $\mathcal{U}^*$ and $\mathcal{W}^*$ from U and W^* with (227) to calculate $\overline{\mathbf{U}}_{\mathbf{1}}$;
- Calculate $\mathbf{s}(\overline{\mathbf{U}}_{\mathbf{1}})$ and $\mathbf{f}(\overline{\mathbf{U}}_{\mathbf{1}})$;
- Compute the second explicit stage as per (180);
- Extract U and W^* from $\mathcal{U}^*$ and $\mathcal{W}^*$ with (228) and (229);
- Compute the second implicit stage with (248), (249) and (250) and extract $\mathcal{U}^*$ and $\mathcal{W}^*$ from U and W^* with (227) to calculate $\overline{\mathbf{U}}^{\mathbf{n+1}}$;

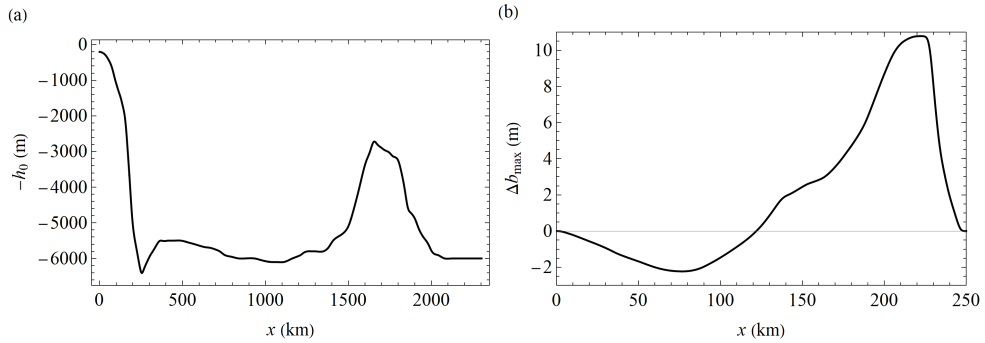

Figure 8: (a) Bathymetry and (b) maximum seabed vertical displacement.

6.2 Numerical results

The model is used to simulate a tsunami generated by an earthquake in a 1D-case. The goal is to assess the effect of compressibility and of the various variants of the equations on the results. This is by no means a simulation of a real tsunami although it is loosely inspired by a simulation of the Tohoku 2011 event by Abdolali & Kirby (2017) who used a seabed motion reconstruction from Grilli *et al.* (2012).

The bathymetry used for the numerical calculations is shown in Figure 8(a) as the variations of $b = -h_0$ with the abscissa x (taking the horizontal datum at the still water level). The domain is 2300 km long with two sponge layers on each side to absorb the waves. The coast is on the left of the figure in the direction of negative abscissas. The sponge layer in this direction has a constant depth of 200 m and 100 cells. The sponge layer on the right of the figure has 200 cells and a constant depth of 6000 m. In some parts of the domain, notably in the oceanic trench for $0 \leqslant x \leqslant 400$ km, the variation of the bottom in space is rapid enough to justify the use of a non-uniform meshing. The minimum size of the cells is 180 m and the maximum size is 1000 m for a total of 2890 cells.

The first test was the "sea at rest". The numerical scheme was found to preserve the equilibrium state, which confirms its well-balanced property.

In the following test, a 1D-tsunami was simulated. The tsunami is initiated by a seabed movement caused by an earthquake. The maximum value $\Delta b_{\max}$ of the variation Δb of the bottom is shown in Figure 8(b). Since no real simulation is intended, the movement of the bottom is supposed to follow the simple function

$$h_0(x,t) = h_0(x,0) - \frac{\Delta b_{\max}(x)}{2}\left(1 + \tanh\frac{t-\tau/2}{\tau_m}\right). \tag{251}$$

Different values of τ and τ_m were used. The most important parameter is τ_m which determines the rapidity of the seabed movement. If τ_m is small ($\tau_m \leqslant 20$ s in the present case), the fast movement of the bottom generates acoustic waves with an important amplitude for the non-hydrostatic pressure although the effect on the water elevation is very small. This is due to the values of $\partial h_0/\partial t$ which are large if τ_m is small. For larger values of τ_m, there is no perceptible acoustic waves generated by the bottom movement. The value of τ must be chosen large enough to give no discontinuity of h_0 at the initial time. The following tests were obtained with the values $\tau_m = 40$ s and $\tau = 600$ s for which there is no generated acoustic waves. Note that, in the cases where there are acoustic waves, they behave as described at the end of §2.7 with, in particular, a cutoff frequency and a reflection on small depths.

The movement of the seabed generates two waves, one propagating toward the coast and another propagating in the opposite direction. These waves at different times (1477 s, 2584 s, 3876 s and 8861 s) are shown on Figure 9. The tsunami propagating shoreward steepens rapidly

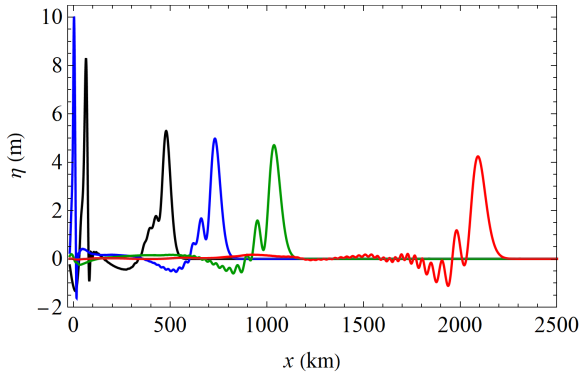

Figure 9: Water elevation at $t = 1477\,\mathrm{s}$ (black), $t = 2584\,\mathrm{s}$ (blue), $t = 3876\,\mathrm{s}$ (green), $t = 8861\,\mathrm{s}$ (red).

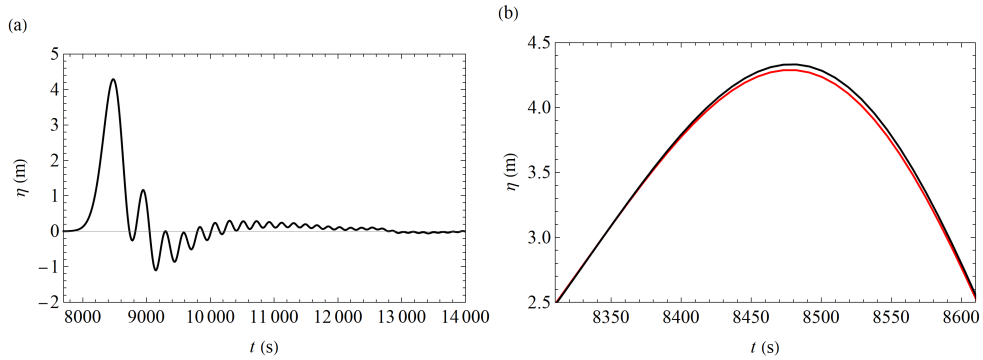

Figure 10: (a) Water elevation as a function of time at $x = 2000\,\mathrm{km}$; (b) Mild-slope equations (black) and equations with an arbitrary bathymetry (red).

and its amplitude increases quickly. In the other wave, a train of secondary waves is generated during the propagation, behind the main hump (Figure 9).

The water elevation at $x = 2000\,\mathrm{km}$ as a function of time is presented in Figure 10(a). A simulation was performed with the mild-slope equations for a comparison to the equations with an arbitrary bathymetry. A comparison around the wave maximum amplitude is presented in Figure 10(b). The difference is about 1 % for the maximum amplitude and is no more than 1 s for the arrival time. The bathymetric terms of $O(\varepsilon^2)$ have thus a very small but not completely negligible effect on the tsunami propagation. On the other hand the mild-slope equations are much simpler and can be used with a good approximation if the slopes are not very steep.

The standard equations are compared to the four-equation system with improved dispersive properties ($\alpha = 1$) and to the five-equation system with $\alpha = 1.19$. The results given for each system (the black, blue and red curves respectively) at $x = 2000\,\mathrm{km}$ as a function of time are presented in Figure 11(a) around the maximum amplitude and in Figure 11(b) in the later part with small secondary waves. In Figure 11(a), the cases $\alpha = 1$ and $\alpha = 1.19$ are practically identical and both have an arrival time which is 3 s shorter than for the standard model and a maximum amplitude approximately 1 % larger. In the latter part, the small secondary waves arrive earlier with $\alpha = 1.19$ than with $\alpha = 1$ which, in turn, arrive earlier than with the standard model.

As was shown in §2.6, the standard model gives an accurate phase velocity for large wavelengths but for shorter waves, the predicted phase velocity is too small. The accuracy domain is increased with the system with improved dispersive properties and $\alpha = 1$ and even more if

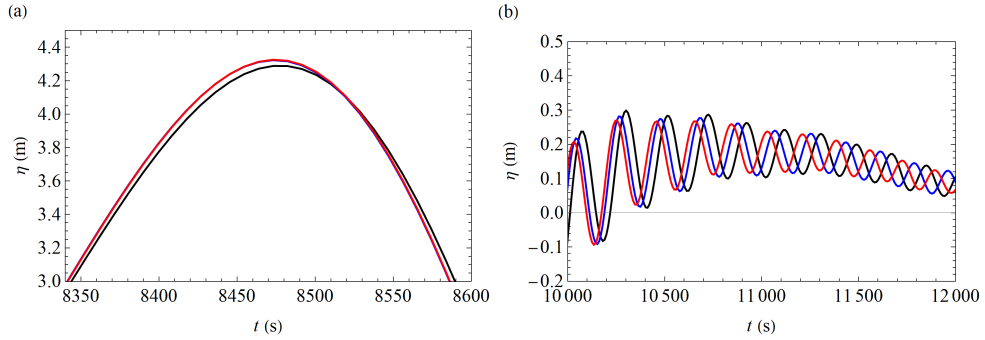

Figure 11: Water elevation at $x = 2000\,\text{km}$ as a function of time for the standard system (black curve), the four-equation system with improved dispersive properties and $\alpha = 1$ (blue curve) and the five-equation system with $\alpha = 1.19$ (red curve). (a) Elevation around the maximum amplitude (the blue curve is indistinguishable from the red curve). (b) Elevation in the later part of the wave train.

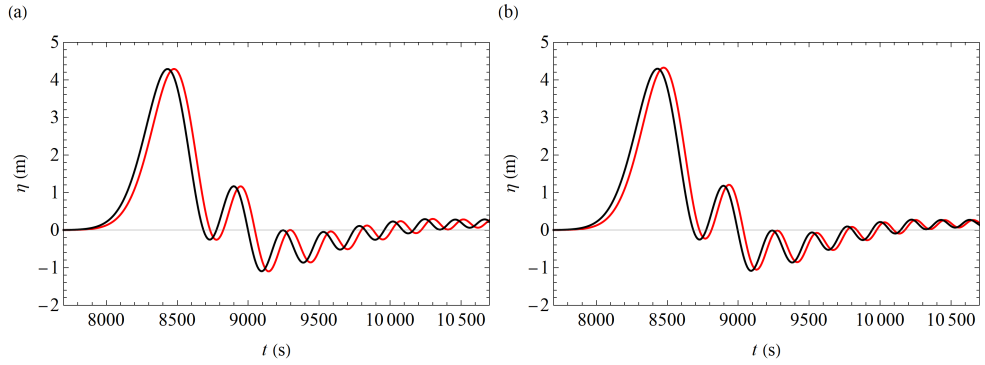

Figure 12: Water elevation at $x = 2000\,\text{km}$ for the compressible case equations (red curve) and the quasi-incompressible case equations (black curve). (a) Standard equations. (b) Equations with improved dispersive properties and $\alpha = 1.19$.

$\alpha = 1.19$. The first waves have the largest wavelengths and are in the domain (kh_0 can be estimated in the 0.3–0.5 range) where the standard system have slightly too small velocities and where the improved system with $\alpha = 1$ is still accurate which explains why the system with $\alpha = 1.19$ gives no improvement (see the deviation of the phase velocity in Figure 3(b)). On the other hand, the later waves are shorter and are in a domain (kh_0 can be estimated in the 0.7–0.9 range) where the standard system gives too small velocities, the improved system with $\alpha = 1$ gives higher values but still too small and where the five-equation system with $\alpha = 1.19$ gives accurate values (see Figure 3(b)). The four-equation model with improved dispersion ($\alpha = 1$) is sufficiently accurate for tsunamis with large wavelengths and has the advantage of an exact energy conservation. If shorter wavelengths are important, the five-equation model with $\alpha = 1.19$ is preferable even though the energy is only asymptotically conserved.

The effect of compressibility is studied by the comparison between the results given by the compressible case equations and by the quasi-incompressible case equations (i.e. $R = Q_0 = Q_1 = Q_2 = 1$ and $R' = Q_1' = M = 0$). The water elevation at $x = 2000\,\text{km}$ is presented in Figure 12(a) for the standard equations and in Figure 12(b) for the system with improved dispersive properties and $\alpha = 1.19$ (in both cases, the compressible case is in red and the quasi-incompressible case in black). For the standard equations, the main wave (maximum amplitude) arrives 46 s later in the compressible case than in the quasi-incompressible case. For the extended

model, the arrival time in the compressible case is 43 s later than in the quasi-incompressible case. These values are very close to the time lag found by Abdolali & Kirby (2017) (48 s) in a similar, although not identical, case. The inclusion of compressibility in the model leads to a significant reduction of the velocity of the tsunami and to an increase of the arrival time.

7 Conclusion

A new structure of equations is obtained for compressible shallow-water flows with a depth-averaging method. The depth-averaged density is variable. Since the shallow-water assumption implies that the system is weakly dispersive, the effect of the non-hydrostatic part of the pressure on the density variations is negligible and the average density variations are due to the variations of the hydrostatic pressure caused by the changes of the water depth.

The equations are derived with a weak-compressibility assumption, from the mass, momentum and energy balance equations. More precisely, the Mach number is supposed to be of $O(\varepsilon^\gamma)$ where ε is the shallow water parameter and $0 < \gamma \leqslant 1$. In the general case of an arbitrary bathymetry as well as in the particular case of a mild-slope bottom, the system is fully nonlinear, hyperbolic, with four equations, and admits an exact energy conservation equation. The linear dispersive properties are consistent with the linear theory of compressible fluids at the long-wave limit. In particular, the compressibility decreases the phase velocity of the gravity waves.

The equations include the case of a mobile bottom to simulate the generation of tsunamis by earthquakes and the vertical movements of the seabed.

To obtain accurate dispersive properties at all tsunamis wavelengths, two methods are used to improve the dispersive properties. The first one is specific to the compressible case and is accurate for tsunamis with long wavelengths such as those generated by earthquakes. This method leads to a four-equation system admitting an exact energy conservation. The second method, which comes in addition to the first one, is an adaptation to the compressible case of the method of Bonneton *et al.* (2011). A fifth variable and a fifth equation are added. The obtained five-equation system is hyperbolic. Its dispersive properties are very accurate for all tsunamis wavelengths including the shorter wavelengths of tsunamis generated by submarine landslides. The drawback of this method, as in the incompressible case, is that the conservation of energy is not satisfied exactly but only asymptotically.

The solutions of the dispersion relation divide into a slow – or hydraulic – branch, governing the usual gravity waves of open-channel hydraulics, and a fast – or acoustic – branch, governing acoustic waves. The acoustic waves are evanescent below a cutoff frequency which increases if the depth decreases. This leads to a reflection of these acoustic waves on regions of small depths. Acoustic waves can be generated by the system if the initial movements of the mobile bottom which generate the tsunami are rapid enough.

In the case of a constant depth, the four-equations systems admit soliton solutions although their profile is found by the numerical resolution of an ordinary differential equation.

The numerical scheme used to solve the system is based on a splitting between a slow part, solved explicitly, and a fast part, solved implicitly. Since the implicit part of the scheme does not involve the resolution of a global linear system, its computational cost is very cheap. The second order in space is obtained with a MUSCL method and the second order in time is obtained with the IMEX ARS2(2,2,2) scheme of Ascher *et al.* (1997). Numerical simulations were obtained, in the case of a constant depth, for a soliton and, in the case of a variable bottom, for a 1D-tsunami generated by a mobile seabed. The equations predict a later arrival time of the tsunami due to compressibility effects.

The importance of these equations are, firstly, that they have a hyperbolic structure which enables a more efficient numerical resolution than the incompressible case which implies an

elliptic step in the numerical scheme, in the same way as the works of Favrie & Gavrilyuk (2017) and Escalante *et al.* (2019), and, secondly, that they include for the first time, real compressible effects in a fully nonlinear depth-averaged system of equations which corresponds, in the compressible case, to the Boussinesq-type family of models in the incompressible case.

This system of equations is a first step toward a complete model for tsunamis, which will need the inclusion, in particular, of the elastic waves in the solid bottom, of the Coriolis forces, and of shearing and possible breaking effects near the coasts, before realistic 2D-applications. This structure of equations can also be used for other shallow-water flows with compressible effects. Granular flows, for example, have often a much smaller sound velocity than water and consequently relatively stronger compressible effects, with density variations in the flow depth. This is also often the case of snow avalanches. These particular flows need specific treatments due to other phenomena, such as a non-Newtonian rheology or thermal effects, but the equations derived in the present paper can be a basic mathematical structure for compressible shallow-water flows.

Funding. The work was supported by the INSU-CNRS (Institut National des Sciences de l'Univers – Centre National de la Recherche Scientifique) program LEFE-MANU (Méthodes Mathématiques et Numériques), project DWAVE.

Declaration of Interests. The author reports no conflict of interest.

A Derivation with an arbitrary bathymetry

In the following, only the differences with the case of a constant bathymetry are presented. The hydrostatic part of the density is

$$\rho_H = \rho_s \mathrm{e}^{g(Z-z)/a^2} \tag{252}$$

and the hydrostatic pressure is then

$$p_H = a^2 \rho_s \left[\mathrm{e}^{g(Z-z)/a^2} - 1 \right]. \tag{253}$$

This changes nothing to the expression of R. The asymptotic expression of the vertical velocity is

$$\tilde{w} = (\tilde{b} - \tilde{z}) \frac{\partial \tilde{U}}{\partial \tilde{x}} + \frac{\partial \tilde{b}}{\partial \tilde{t}} + \tilde{U} \frac{\partial \tilde{b}}{\partial \tilde{x}} + O(\varepsilon^{\beta}) + O(\varepsilon^{2\gamma}) \tag{254}$$

with the depth-averaged vertical velocity

$$\tilde{W} = -\frac{\tilde{h}}{2} \frac{\partial \tilde{U}}{\partial \tilde{x}} + \frac{\partial \tilde{b}}{\partial \tilde{t}} + \tilde{U} \frac{\partial \tilde{b}}{\partial \tilde{x}} + O(\varepsilon^{\beta}) + O(\varepsilon^{2\gamma}). \tag{255}$$

Defining $w' = w - W$, we obtain the consistent expression

$$\overline{w'^2} \simeq \frac{h^2}{12} \left(\frac{\partial U}{\partial x} \right)^2 \simeq \frac{1}{3} \left(W - \dot{b} \right)^2. \tag{256}$$

The consistent expression of the non-hydrostatic pressure at the bottom is

$$p_N(b) \simeq -\frac{h^2}{2} \left[\frac{\partial^2 U}{\partial x \partial t} + U \frac{\partial^2 U}{\partial x^2} - \left(\frac{\partial U}{\partial x} \right)^2 \right] + h\ddot{b} \tag{257}$$

and the depth-averaged non-hydrostatic pressure writes

$$P \simeq -\frac{h^2}{3}\left[\frac{\partial^2 U}{\partial x \partial t} + U\frac{\partial^2 U}{\partial x^2} - \left(\frac{\partial U}{\partial x}\right)^2\right] + \frac{h}{2}\ddot{b}. \tag{258}$$

The quantity $p_N(b)$ appears in the depth-integrated momentum balance equation in the Oz-direction and, in the case of an arbitrary bathymetry, in the Ox-direction too. In the first case, the expression

$$p_N(b) = \frac{3}{2}P + \frac{h}{4}\ddot{b} \tag{259}$$

is used, while in the second case $p_N(b)$ is expressed as

$$\tilde{p}_N(b) = 2\tilde{P} + \frac{\tilde{h}}{3}\frac{\mathrm{D}}{\mathrm{D}\tilde{t}}\left(\frac{\mathrm{D}\tilde{b}}{\mathrm{D}\tilde{t}} - \tilde{W}\right) + O(\varepsilon^{2\gamma}) + O(\varepsilon^{\beta}). \tag{260}$$

These expressions lead to the equations (192) and (195).

References

Abdolali, A., Kadri, U. & Kirby, J. T. 2019 Effect of water compressibility, sea-floor elasticity, and field gravitational potential on tsunami phase speed. *Sci. Rep.* **9**, 1–8.

Abdolali, A. & Kirby, J. T. 2017 Role of compressibility on tsunami propagation. *J. Geophys. Res.-Oceans* **122**, 9780–9794.

Allgeyer, S. & Cummins, P. 2014 Numerical tsunami simulation including elastic loading and seawater density stratification. *Geophys. Res. Lett.* **41**, 2368–2375.

Ascher, U. M., Ruuth, S. J. & Spiteri, R. J. 1997 Implicit-Explicit Runge-Kutta methods for time-dependent partial differential equations. *Appl. Numer. Math.* **25**, 151–167.

Auclair, F., Bordois, L., Dossmann, Y., Duhaut, T., Paci, A., Ulses, C. & Nguyen, C. 2018 A non-hydrostatic non-Boussinesq algorithm for free-surface ocean modelling. *Ocean. Model.* **132**, 12–29.

Baba, T., Allgeyer, S., Hossen, J., Cummins, P. R., Tsushima, H., Imai, K., Yamashita, K. & Kato, T. 2017 Accurate numerical simulation of the far-field tsunami caused by the 2011 Tohoku earthquake, including the effects of Boussinesq dispersion, seawater density stratification, elastic loading, and gravitational potential change. *Ocean Model.* **111**, 46–54.

Bonneton, P., Chazel, F., Lannes, D., Marche, F. & Tissier, M. 2011 A splitting approach for the fully nonlinear and weakly dispersive Green-Naghdi model. *J. Comput. Phys.* **230**, 1479–1498.

Boussinesq, J. 1872 Théorie des ondes et des remous qui se propagent le long d'un canal rectangulaire horizontal, en communiquant au liquide contenu dans ce canal des vitesses sensiblement pareilles de la surface au fond. *J. Mathématiques Pures et Appliquées. Deuxième Série* **17**, 55–108.

Bristeau, M.-O., Mangeney, A., Sainte-Marie, J. & Seguin, N. 2015 An energy-consistent depth-averaged Euler system: derivation and properties. *Discrete Cont. Dyn.-B* **20**, 961–988.

Brocchini, M. 2013 A reasoned overview on Boussinesq-type models: the interplay between physics, mathematics and numerics. *Proc. R. Soc. A* **469**, 20130496.

Chazel, F., Lannes, D. & Marche, F. 2011 Numerical simulation of strongly nonlinear and dispersive waves using a Green-Naghdi model. *J. Sci. Comput.* **48**, 105–116.

Dalrymple; R. A. & Rogers, B. D. 2007 A note on wave celerities on a compressible fluid. *Coastal Engineering 2006*, 3–13.

Duchêne, V. 2019 Rigorous justification of the Favrie-Gavrilyuk approximation to the Serre-Green-Naghdi model *Nonlinearity* **32**, 3772.

Duran, A. & Marche, F. 2017 A discontinuous Galerkin method for a new class of Green-Naghdi equations on simplicial unstructured meshes *Appl. Math. Model.* **45**, 840–864.

Escalante, C., Dumbser, M. & Castro, M.J. 2019 An efficient hyperbolic relaxation system for dispersive non-hydrostatic water waves and its solution with high order discontinuous Galerkin schemes. *J. Comput. Phys.* **394**, 385–416.

Escalante, C. & Morales de Luna, T. 2020 A general non-hydrostatic hyperbolic formulation for Boussinesq dispersive shallow flows and its numerical approximation. *J. Sci. Comput.* **83**, 1–37.

Favrie, N. & Gavrilyuk, S. 2017 A rapid numerical method for solving Serre-Green-Naghdi equations describing long free surface gravity waves. *Nonlinearity* **30**, 2718–2736.

Gavrilyuk, S., Ivanova, K. & Favrie, N. 2018 Multi-dimensional shear shallow water flows: Problems and solutions. *J. Comput. Phys.* **366**, 252–280.

Giraldo, F. X., Kelly, J. F. & Constantinescu, E. M. 2013 Implicit-Explicit formulations of a three-dimensional nonhydrostatic unified model of the atmosphere (NUMA). *SIAM J. Sci. Comput.* **35**, B1162–B1194.

Green, A. E., Laws, N. & Naghdi, P. M. 1974 On the theory of water waves. *P. Roy. Soc. Lond. A Mat.* **338**, 43–55.

Green, A. E. & Naghdi, P. M. 1976 A derivation of equations for wave propagation in water of variable depth. *J. Fluid Mech.* **78**, 237–246.

Grilli, S. T., Harris, J. C., Tajalli Bakhsh, T., Masterlark, T. L., Kyriakopoulos, C., Kirby, J. T. & Shi, F. 2012 Numerical simulation of the 2011 Tohoku tsunami based on a new transient FEM co-seismic source: Comparison to far- and near-field observations. *Pure Appl. Geophys.* **170**, 1333–1359.

Hill, G. E. 1974 Factors controlling the size and spacing of cumulus clouds as revealed by numerical experiments. *J. Atmos. Sci.* **31**, 646–673.

Kadri, U. 2015 Wave motion in a heavy compressible fluid: Revisited. *Eur. J. Mech. B-Fluids* **49**, 50–57.

Kazakova, M. & Richard, G. L. 2019 A new model of shoaling and breaking waves: One-dimensional solitary wave on a mild sloping beach. *J. Fluid Mech.* **862**, 552–591.

Kennedy, A. B., Kirby, J. T., Chen, Q., & Dalrymple, R. A. 2001 Boussinesq-type equations with improved nonlinear performance. *Wave Motion* **33**, 225–243.

Kirby, J. T. 2016 Boussinesq models and their application to coastal processes across a wide range of scales. *J. Waterw. Port Coast.* **142**, 03116005.

Kirby, J. T., Shi, F., Tehranirad, B., Harris, J. C. & Grilli, S. T. 2013 Dispersive tsunami waves in the ocean: Model equations and sensitivity to dispersion and Coriolis effects. *Ocean Model.* **62**, 39–55.

Klemp, J. B. & Wilhelmson, R. B. 1978 The simulation of three-dimensional convective storm dynamics. *J. Atmos. Sci.*. **35**, 1070–1096.

Lannes, D. 2013 *The Water Waves Problem: mathematical analysis and asymptotics.* Mathematical Surveys and Monographs, vol. **188**, Amer. Math. Soc., Providence.

Liang, Q. & Marche, F. 2009 Numerical resolution of well-balanced shallow water equations with complex source terms. *Adv. Water Resour.* **32**, 873–884.

Madsen, P. A. & Sørensen, O. R. 1992 A new form of the Boussinesq equations with improved linear dispersion characteristics. Part II: a slowly varying bathymetry. *Coast. Eng.* **18**, 183–204.

Mesinger, F. 1977 Forward-Backward Scheme, and its Use in a Limited Area Model. *Contrib. Atmos. Phys.* **50**, 200–210.

Myers, M. 1986 Generalization and extension of the law of acoustic energy conservation in a nonuniform flow. In *24th Aerospace Sciences Meeting*, 471.

Nwogu, O. 1993 Alternative form of Boussinesq equations for nearshore wave propagation. *J. Waterw. Port Coast.* **119**, 618–638.

Pareschi, L. & Russo, G. 2005 Implicit-Explicit Runge-Kutta schemes and applications to hyperbolic systems with relaxation. *J. Sci. Comput.* **25**, 129–155.

Peregrine, D. H. 1967 Long waves on a beach. *J. Fluid Mech.* **27**, 815–827.

Pidduck, F. B. 1910 On the propagation of a disturbance in a fluid under gravity. *Proc. R. Soc. A* **83**, 347–356.

Serre, F. 1953 Contribution à l'étude des écoulements permanents et variables dans les canaux. *La Houille Blanche* **8**, 374–388.

Skamarock, W. C. & Klemp, J. B. 1992 The stability of time-split numerical methods for the hydrostatic and the nonhydrostatic elastic equations. *Mon. Weather Rev.* **120**, 2109–2127.

Skamarock, W. C. & Klemp, J. B. 2008 A time-split nonhydrostatic atmospheric model for weather research and forecasting applications. *J. Comput. Phys.* **227**, 3465–3485.

Stelling, G. & Zijlema, M. 2003 An accurate and efficient finite-difference algorithm for non-hydrostatic free-surface flow with application to wave propagation *Int. J. Numer. Meth. Fl.* **43**, 1–23.

Su, C. H. & Gardner, C. S. 1969 Korteweg-de Vries equation and generalizations, III. Derivation of the Korteweg-de Vries equation and Burgers equation. *J. Math. Phys.* **10**, 536–539.

Tappin, D. R., Grilli, S. T., Harris, J. C., Geller, R. J., Masterlark, T., Kirby, J. T., Shi, F., Ma, G., Thingbaijam, K. K. S. & Mai, P. M. 2014 Did a submarine landslide contribute to the 2011 Tohoku tsunami ? *Mar. Geol.* **357**, 344–361.

Tkachenko, S. 2020 Étude analytique et numérique d'un modèle dispersif des eaux peu profondes. PhD thesis, Université d'Aix-Marseille.

Teshukov, V. M. 2007 Gas-dynamics analogy for vortex free-boundary flows. *J. Applied Mechanics and Technical Physics* **48**, 3, 303–309.

Tsai, V. C., Ampuero, J.-P., Kanamori, H., Stevenson, D. J. 2013 Estimating the effect of Earth elasticity and variable water density on tsunami speeds. *Geophys. Res. Lett..* **40**, 492–496.

Walters, R. A. 2005 A semi-implicit finite element model for non-hydrostatic (dispersive) surface waves. *Int. J. Numer. Meth. Fl.* **49**, 721–737.

Watada, S. 2013 Tsunami speed variations in density-stratified compressible global oceans. *Geophys. Res. Lett.* **40**, 4001–4006.

Watada, S., Kusumoto, S., & Satake, K. 2014 Traveltime delay and initial phase reversal of distant tsunamis coupled with the self-gravitating elastic Earth. *J. Geophys. Res.-Sol. Ea.* **119**, 4287–4310.

Wei, G., Kirby, J. T., Grilli, S. T. & Subramanya, R. 1995 A fully nonlinear Boussinesq model for surface waves. Part I: highly nonlinear unsteady waves. *J. Fluid Mech.* **294**, 71–92.

Weller, H., Lock, S.-J. & Wood, N. 2013 Runge-Kutta IMEX schemes for the horizontally Explicit/Vertically Implicit (HEVI) solution of wave equations. *J. Comput. Phys.* **252**, 365–381.

Whitham, G. B. 1974 *Linear and Nonlinear Waves.* Wiley.

Yamazaki, Y., Cheung, K. F., & Kowalik, Z. 2011 Depth-integrated, non-hydrostatic model with grid nesting for tsunami generation, propagation, and run-up. *Int. J. Numer. Meth. Fl.* **67**, 2081–2107.